2.10. Tumor suppression efficacy

BALB/c nude mice were inoculated subcutaneously with BxPC3 cells derived from human pancreatic adenocarcinoma (1×10^7 cells in 100 μL of PBS). Tumors were allowed to grow for 10 days until proliferative phase (tumor size was approximately 75 mm^3). Then 200 μL of each polyplex micelle solution [20 μg soluble fms-like kinase-1 (sFlt-1) pDNA/mouse] in 10 mM HEPES buffer (pH 7.4) with 150 mM NaCl was intravenously injected through the tail vein thrice on days 0, 4 and 8. Tumor size was measured every two or three days with a digital vernier caliper across its longest (a) and shortest diameters (b), and its volume (V) was calculated according to the formula $V = 0.5\ ab^2$. The tumor size measurement was discontinued when the tumors in the control group showed ulcer characteristics according to the guideline for animal experiments. Tumor progression was evaluated in terms of relative tumor volume to day 0 (day for the first polyplex micelle injection), $n = 6$.

2.11. Vascular density

Each polyplex micelle loading sFlt-1 (20 μg of pDNA in 200 μL HEPES buffer containing 150 mM NaCl) was intravenously injected into the BxPC3 tumor-bearing mice through the tail vein on days 0 and 4. Mice were sacrificed on day 6, and the tumors were excised, frozen in dry-iced acetone, and sectioned into 20 μm thick slices with a cryostat. Vascular endothelial cells (VECs) were immunostained with rat monoclonal antibody antiplatelet endothelial cell adhesion molecule-1 (PECAM-1) (BD Pharmingen, Franklin Lakes, NJ), followed by incubation with Alexa Fluor 488-conjugated secondary antibody. The immunostained sections were observed with CLSM780 (Carl Zeiss, Germany). The vascular density was quantified by counting the percentage area of PECAM-1-positive pixels per image with 12 images per sample.

2.12. sFlt-1 expression at the tumor site

Each polyplex micelle loading sFlt-1 (20 μg of pDNA in 200 μL HEPES buffer containing 150 mM NaCl) was intravenously injected into the BxPC3 tumor-bearing mice *via* the tail vein. Mice were sacrificed at 48 h after injection. The tumors were excised, frozen in dry-iced acetone, and sectioned into 10 μm thick slices with a cryostat. VECs were immunostained using the antibodies anti-mouse PECAM-1 (BD Pharmingen, San Diego, CA) and anti-human and mouse VEGFR1 (ab32152, Abcam Japan, Tokyo, Japan). The sections immunostained was observed with CLSM780 (Carl Zeiss, Germany). The sFlt-1 gene expression was quantified by counting the integral fluorescence intensity of ab32152-positive pixels per image with six images per sample.

2.13. Tumor accumulation

Mice bearing BxPC3 tumor with similar tumor volume of approximate 700 mm^3 were randomly selected for each cohort ($n = 9$). Polyplex micelles of 200 μL of solution prepared from Cy5-labeled pDNA were intravenously injected into the blood stream through the tail vein to quantify the tumor accumulation of polyplex micelles. Mice were sacrificed 24 h after injection. The tumor tissue was excised. The lysed solution of tumor tissue was dispensed into 96-well opaque plate and the corresponding Cy5 fluorescence was measured by IVIS® Lumina II (Caliper Life Sciences, Hopkinton, MA). The results were expressed as total photon counts normalized by tumor weight.

2.14. Statistical analysis

The *p* values were determined by the Student's *t*-test using a two-tailed distribution and two-sample un-equal variance with the T. Test function of Microsoft Excel. The *p* values of less than 0.05 were considered as statistically significant.

3. Results and discussion

3.1. Polymer synthesis and characterizations of polyplex micelles

PEG-PAsp(DET)-cholesteryl was synthesized by conjugation of cholesteryl group to precursor PEG-PBLA), followed by aminolysis reaction with DET. For the synthesis of cRGD-PEG-PAsp(DET)-cholesteryl, acetal-PEG-NH_2 was used as the starting material for polymerization according to a similar synthetic procedures, yielding acetal-PEG-PAsp(DET)-cholesteryl. Then the acetal group in this product was activated at acidic pH for reaction with the cRGD peptide to yield cRGD-PEG-PAsp(DET)-cholesteryl (Supporting Information, Scheme S1). The resulting block copolymers were characterized by ^1H NMR and GPC measurement (Supporting Information Fig. S1, S2 and S3) and the chemical descriptions are summarized in Table 1.

For preparation of polyplex micelles, each polymer product listed in Table 1 was dissolved in 10 mM HEPES buffer (pH 7.4), followed by mixing with pDNA solution at varying N/P ratios. The abbreviations for each polyplex micelle are listed in Table 1. The sizes of the polyplex micelles were measured by dynamic light scattering (DLS) measurement and all the samples presented cumulant diameters ranging from 80 nm to 100 nm with unimodal size distributions of a low polydispersity index (PDI) of ~0.1 (Supporting Information, Table S1).

3.2. In vitro evaluation for polyplex micelles

For enhancing PEG shielding to confer prolonged blood retention on polyplex micelles, we attempted to increase the M_w of PEG in the block copolymer from previously used 12 kDa to 20 kDa. To evaluate its effect on enhanced PEG shielding, we first evaluated cellular uptake activity. Given that the enhanced PEG shielding tends to reduce interactions with biological structures (e.g. cell membrane so as for reduced cell uptake activity [18]), the cellular uptake can be an indicator for PEG shielding. Herein, pDNA labeled with fluorescence dye was used to prepare polyplex micelles, and the cellular uptake efficiency in HeLa cells was quantified by measurement of the fluorescence intensity of internalized pDNA by flow cytometry. The result (Fig. 1a) confirmed a low cellular uptake profile for PEG20C, indicating enhanced PEG shielding. In contrast, the higher cellular uptake for PEG12C implied insufficient PEG shielding.

To address the dilemma of PEG shielding for the reduced cellular uptake, a ligand molecule (cRGD peptides) was strategically conjugated at the distal end of PEG segment in the block copolymer intended for promoting specific ligand-integrin-mediated uptake. Our previous study showed that the benefits of ligand conjugation were particularly pronounced for the polyplex micelles with high PEG shielding, where non-specific interaction was minimized so that cRGD-integrin mediated affinity elicited and mediated efficient gene expression activity in the transfected cells [18]. We accordingly expected that R-PEG20C with its high PEG shielding effect would offer the prospect of fully exploiting benefits of ligand-integrin mediated affinity. Because HeLa cells with over-expression of cRGD specific integrins ($\alpha_V\beta_3$ and $\alpha_V\beta_5$) on the cell surface [18], cellular uptake and subsequent gene expression of polyplex micelles were examined to verify the cRGD effect. R-PEG20C showed a marked increase in contrast to low uptake level of PEG20C (Fig. 1a), indicating the benefit of cRGD in promoting cellular uptake.

Elevated gene expression was also observed in reporter gene expression evaluation, where gene expression level of R-PEG20C exhibited one order of magnitude higher than that of PEG20C (Fig. 1b). It is noteworthy that this higher expression was observed despite the lower cellular uptake activities shown by R-PEG20C compared with PEG12C (Fig. 1a). To this regard, gene expression activity was normalized by cellular uptake to yield transfection efficiency (Fig. 1c). R-PEG20C exhibited markedly higher transfection efficiency than PEG12C and PEG20C, in particular R-PEG20C at an N/P ratio of 8 presented the highest transfection efficiency (N/P 8 was accordingly chosen for hereafter biophysical evaluation and therapeutic trials). The high transfection efficiency of R-PEG20C implied that the cRGD motif may confer benefits not only for cellular uptake but also for the post-endocytosis process (intracellular trafficking). For the ligand-free polyplex micelle system [cRGD(−)], the internalized polyplex micelles after endocytosis are subjected to endosome entrapment, eventually resulting in enzymatic degradation if they cannot afford adequate facilities to retrieve the entrapped polyplex micelles from late endosome. In this respect, the colocalization of polyplex micelle with digestive

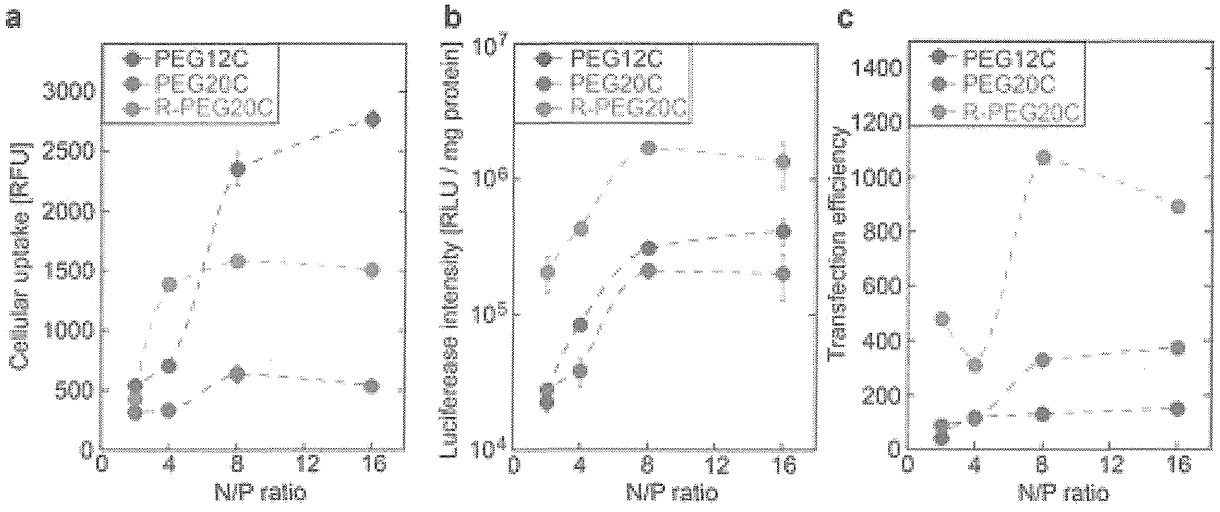

Fig. 1. Cellular uptake and gene expression activity of polyplex micelles at varying N/P ratios in HeLa cells. (a): Cellular uptake (mean ± SEM, $n = 3$). (b): Gene expression activity (mean ± SEM, $n = 4$). (c): Normalized transfection efficiency obtained from dividing gene expression activity by cellular uptake activity.

late endosome and lysosome was quantified for each sample. It should be noted that the cationic segment of PAsp(DET) affords escape capacity from acidic endosome entrapment: PAsp(DET) featured as the functional flanking ethylenediamine moiety in the side chain of N-substituted polyaspartamide (PAsp), exhibits distinctive two-step protonation behavior in response to a pH gradient, where the protonation of ethylenediamine is stimulated from single protonation (pH 7.4) to double protonation (90% at pH 5) [8]. This acid-responsive trait of PAsp(DET) results in a selective endosome membrane destabilization function, consequently led to liberation of embedded polyplex micelles from endosome entrapment to the cytosol. To gain clear insight on intracellular trafficking of polyplex micelles, CLSM observation was carried out to distinguish their intracellular distribution (Fig. 2). Herein, pDNA was labeled with Cy5 (red) and digestive late endosome/lysosomes were labeled by LysoTracker Green (green). Therefore, intracellular yellow pixels (colocalization) represent entrapment of polyplex micelles in the late-endosome/lysosome compartment, whereas intracellular red pixels (non-colocalization) indicate their presence in the cytosol. Accordingly, a lower colocalization degree indicates lower entrapment of polyplex micelles in the acidic digestive compartment. Fig. 2d reveals that the samples of PEG12C and PEG20C showed a colocalization ratio of approximately 60%, confirming efficient endosome escape capacity presumably by virtue of the functionalities of PAsp(DET). It is noteworthy that colocalization ratios of R-PEG20C appeared to be much lower than others. To this issue, the previous study suggested possibility of alternative pathway for intracellular trafficking after cRGD-mediated uptake, featured with rapid migration to the nucleus proximity in the cytosol in clear comparison of cRGD(−) micelle [24]. Thus, R-PEG20C may follow a favorable intracellular trafficking pathway avoiding entrapment in digestive compartments and thereby mediating dramatically high gene expression efficiency.

Although the cellular uptake level of PEG20C was much lower than PEG12C, the normalized transfection efficiency of PEG20C was higher than PEG12C. In view of their comparable endosome escape activity, we suspected that the pDNA encapsulated within PEG12C may have been damaged to some extent, whereas it was more protected in PEG20C. To investigate this hypothesis, the tolerance of polyplex micelle to DNase I digestion was evaluated by quantifying the remaining percentage of intact functional DNA (including supercoiled, open-circular and linear DNA, the transcriptionally active forms), revealing better tolerance by PEG20C than by PEG12C (Supporting Information Fig. S4). This superiority may be explained by the higher shielding effect of PEG20C than that of PEG12C, such that the accessibility of digestive enzyme to encapsulated pDNA is reduced, permitting the transport of more intact DNA into the nucleus.

3.3. PEG shielding and blood retention property

As described above, improved PEG shielding for polyplex micelle was achieved by elongation of the PEG segment from 12 kDa to 20 kDa. To characterize quantitatively the PEG surface shielding for polyplex micelles, we calculated the PEG density for polyplex micelles of PEG20C and PEG12C. To evaluate the cholesteryl effect on formulating the polyplex micelle, we included a control PEG12 sample without the cholesteryl moiety. For estimation of PEG density, the surface area of the complex core, representing the area available for PEG tethering, was the first requirement to be determined because the PEG density is expressed as the number of tethered PEG chains per unit area available for PEG (the core surface area). With this purpose, the morphology of polyplex micelles was characterized by transmission electron microscopy (TEM) measurement. Note that pDNA in polyplex micelles were selectively observed in the TEM image owing to stronger affinity of uranyl acetate (staining agent) to DNA than PEG. All polyplex micelles appeared as uniform rod-shaped particles (Fig. 3), suggesting that pDNA is packaged into the rod-shaped bundle through a regular folding behavior [25]. Assuming the bundle to be a cylindrical structure, the surface area of the complex core (Table 2) can be calculated by the surface area of the cylinder side plus the area of both of its ends (a detailed calculation was described in Supporting Information). The number of tethered PEG chains in the polyplex micelle is another requirement for determining the tethered PEG density, which was determined from ultracentrifuge analysis as previously reported (Table 2) [23]. The average PEG tethering density $<\sigma>$ was then calculated in terms of the number of PEG chains per unit area (chains/nm^2) (Table 2). Considering that different M_w of PEG (12 kDa and 20 kDa) were used in this PEG density analysis, the normalized PEG density, namely reduced tethering PEG density (RTD), defined as the number of chains that occupy an area covered by an unperturbed polymer chain, was used to characterize PEG tethering density,

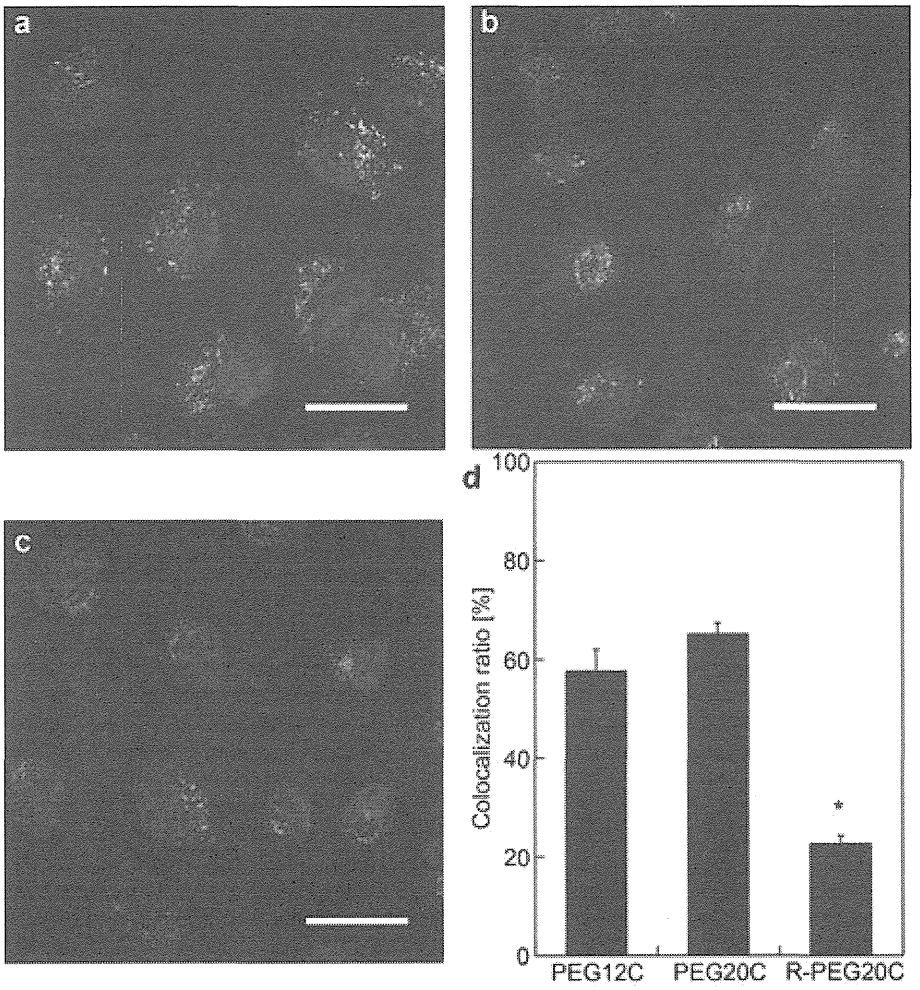

Fig. 2. Confocal laser scanning microscopy (CLSM) observation for intracellular trafficking. (a): PEG12C; (b): PEG20C; and (c): R-PEG20C. Blue: nucleus; Green: late endosome or lysosome; Red: pDNA. Endosome entrapment was determined by quantifying colocalization ratio of pDNA and late endosome/lysosome as summarized in (d) (mean ± SEM, $n = 10$). The scale bars represent 20 μm in all CLSM images.

$$\mathrm{RTD} = \sigma\pi R_g^2$$

where the R_g (radius of gyration of an unperturbed PEG chain) of 12-kDa and 20-kDa PEG were calculated to be 4.7 nm and 6.3 nm, respectively [26,27].

The quantified PEG density in RTD (Table 2) displayed the order PEG12 < PEG12C < PEG20C, which corroborating the effect of cholesteryl conjugation and PEG elongation from 12 kDa to 20 kDa on elevating PEG density in terms of RTD.

Noteworthy is that cholesteryl conjugation (in comparison of PEG12 and PEG12C) appears to promote a markedly increased number of block copolymers bound to pDNA (Table 2). As for PEG12 formulation, approximately 160 chains of PEG12 polymer were bound to each pDNA (Table 2). Given that the polymerization degree of the PAsp(DET) segment of PEG12 polymer is 56 (Table 1) and two amino groups reside in one ethylenediamine unit, these 160 block copolymers accounts for a total of 16,960 (=2 × 160 × 56) amino groups. With 53% of amino groups of PAsp(DET) presumed to be positively charged at pH 7.4 [8], these 16,960 amino groups would account for 8989 (=16960 × 0.53) positive charges at pH 7.4, coinciding reasonably well with the number of negative charge from phosphate groups in one pBR322 (pBR322: 8722 negative charges from 4361 bp). The charge ratio (+/−) of PEG12 formulation is thus calculated to be 1.03 (8989/8722), suggesting a formulation following stoichiometric charge ratio.

In contrast to PEG12, cholesteryl-conjugated PEG12C and PEG20C polymers exhibited considerably larger numbers of block copolymers associating with pDNA. This difference is possibly due to the hydrophobic nature of the cholesteryl moiety. Presumably, block copolymers with hydrophobic cholesteryl conjugation prefer to incorporate into the hydrophobic complex core, rather than staying in aqueous solution, so that a larger number of block copolymers, exceeding the stoichiometric charge ratio, may bind to pDNA. The cholesteryl conjugation also affected the packaging structure of pDNA in the polyplex micelle. The rod length of PEG12C was observed to be shortened from 78.6 nm to 55.8 nm compared with non-cholesteryl PEG12 polyplex micelles (Fig. 3d and e). Presumably the hydrophobic cholesteryl moiety associated with the complex core caused surface energy to increase, and the developed additional compaction force stimulated DNA to more condense for minimizing contact area to water molecules. Eventually, the reduced PEG tethering area could contribute to increase crowdedness of PEG palisade. These results verified worthy strategy of using cholesteryl conjugation to compact packaged DNA more and promote PEG to be further crowding.

In addition, PEG molecular weight also affected the pDNA packaging structure, as found that PEG20C (Fig. 3f) exhibited a longer rod particle than PEG12C (Fig. 3e). It is possible that the

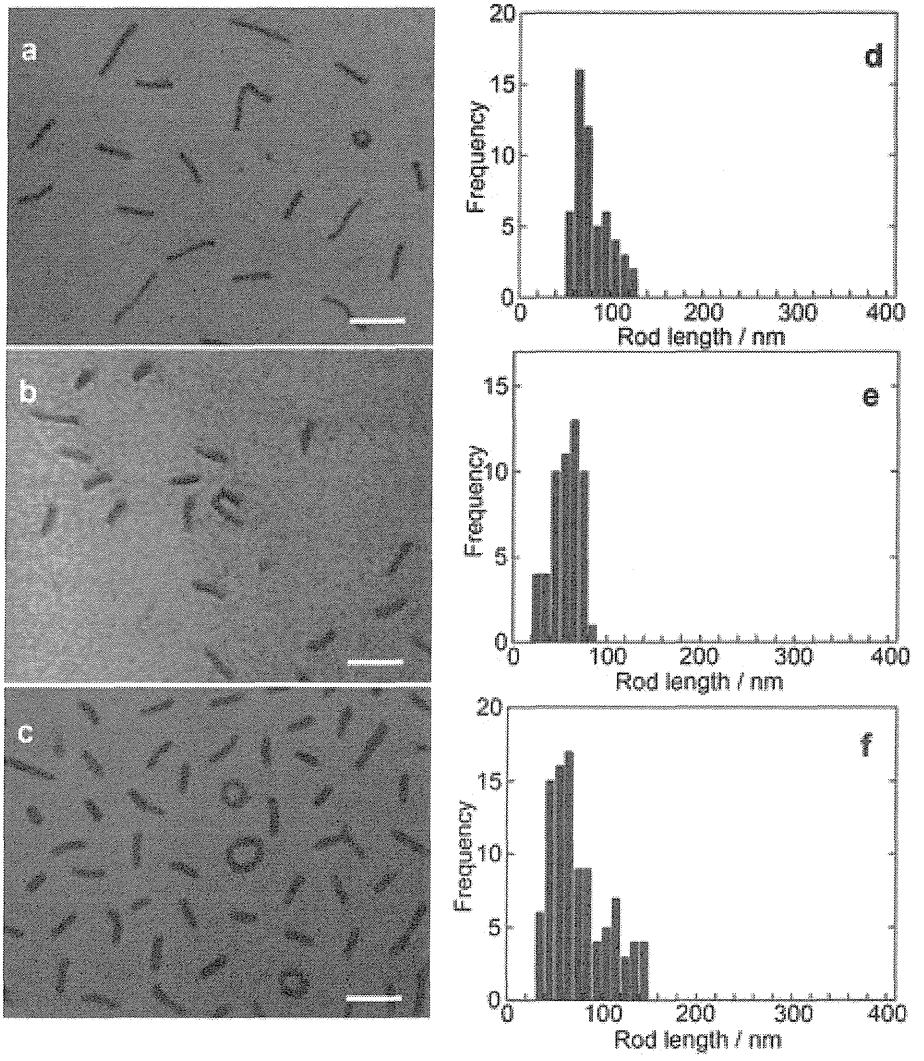

Fig. 3. Morphology and rod length distribution of polyplex micelles according to TEM observation. Representative TEM images of polyplex micelles, (a): PEG12; (b): PEG12C; and (c): PEG20C. Scale bar: 100 nm. Rod length distribution of polyplex micelles analyzed according to acquired TEM images, (d): PEG12; (e): PEG12C; and (f): PEG20C, $n > 100$.

steric repulsion resulting from the higher PEG crowding of PEG20C prevents a form as compact as that of PEG12C. Moreover, the polyplex micelle formulated from 20-kDa PEG showed a slightly smaller number of block copolymers bound to pDNA than the micelle of PEG12C (Table 2). Presumably, the larger steric repulsion of 20-kDa PEG may limit further association to the polyplex micelles likewise 12-kDa PEG, implying that the PEG in PEG20C is already in a substantially crowded state. In summary, the synergistic effect of cholesteryl conjugation was identified; facilitating a larger number of polymers bound to pDNA (over-stoichiometry) and inducing more condensation of pDNA, which eventually resulted in an elevated tethered PEG density. Elongation of the PEG from 12 kDa to 20 kDa also contributed to increased PEG crowdedness. Noteworthy is the crowdedness of PEG palisade predicted from the RTD value (Table 2). According to our previous study on correlation of RTD and PEG conformation [16], the PEG conformation of PEG12 adopted mushroom with overlapped by neighboring PEG chains, whereas that of PEG12C adopted a squeezed conformation. The RTD of PEG20C indicated the PEG conformation adopting further squeezed, even possibly to scalable brush region [17]. As we demonstrated in previous work, PEG modulation to a squeezed conformation increased blood circulation as compared to that of mushroom conformation [17], it is anticipated PEG20C with the elevated PEG crowdedness should afford better stealth function.

Table 2
Characterizations of polyplex micelles for reduced tethered PEG density estimation.

	Aver. Rod length [nm]	Binding number of block copolymers per DNA	Binding [+/−][a]	Density [chains/nm^2]	RTD[b]
PEG12	78.6	160.5	1.03	0.0391	2.68
PEG12C	55.8	298.0	2.17	0.0836	5.74
PEG20C	75.5	238.9	1.77	0.0592	7.39

[a] Binding [+/−]: molar ratio of positive charge from bound block copolymers to negative charge from pDNA.
[b] RTD: reduced tethering PEG density.

The effect of enhanced PEG crowdedness on the blood retention of polyplex micelles was then evaluated. (Note that the blood circulation profile of PEG12 without cholesteryl moiety was not determined because we had previously shown its low blood retention after systemic administration [16].) In brief, following intravenous administration of polyplex micelles into the bloodstream, the blood was collected at appropriate time points and the remaining pDNA in the blood was quantified according to RT-PCR measurement. Note that the method based on PCR more directly

estimates the blood retention because the PCR detects the quantity of intact pDNA (at least primer region). As shown in Fig. 4a, PEG20C showed appreciably increased retention life in the blood circulation compared with PEG12C, which validated PEG elongation as an effective strategy for prolonging blood circulation. The promotion of PEG shielding appeared to be particularly pronounced at the early stage of circulation. Extrapolation of the decay curve to the starting time (0 min) for PEG20C profiles provided approximately 100%, which was contrasted to approximately 10% for PEG12C, suggesting that polyplex micelles of PEG20C, managed to overcome the rapid elimination from the circulation following injection. Most likely, the elevated PEG crowdedness of PEG20C afforded this stealth function to escape from the rapid blood elimination, possibly RES capture initiated by opsonization. It should be noted that tethered PEG with a scalable brush conformation has reported to entirely prohibit large biomolecules (>10 nm) adsorption [28,29], such as opsonins, supporting reasonability of above scheme. However, despite accomplishment to avoid the rapid blood clearance by PEG20C, the retention was not sustained. Instead, the profiles decreased showing similar decay curve with PEG12C, implying that the polyplex micelles were eliminated by the same mode irrespective of the PEG crowdedness. Possibly, the PEG shielding of PEG20C was still inadequate to afford as an effective barrier to prevent relatively small biomolecules, such as nucleases with approximate size of several nanometers [30]. The polyplex micelle received DNase attack for digestion of the encapsulated DNA, resulting in the destabilization of polyplex structure to become more susceptible to dissociation particularly when passing anionic abundant sites or structures, e.g. by heparan sulfate in glomerular basement membrane [31]. Therefore, further efforts will be needed to develop a strategy to resolve this issue for pursuing persistence in the bloodstream. Yet, the effort to promote PEG crowdedness by cholesteryl conjugation, which offered synergistic effect on increase of PEG density in the form of increased tethering PEG chains on more compacted polyplex core, together with PEG elongation, resulted in an appreciable crowded palisade, possibly, scalable brush region, eventually affording a stealth character to escape the rapid elimination after the injection. Of note, further evaluation of blood circulation profile of R-PEG20C confirmed its prolonged retention activities comparable to PEG20C (Fig. S5), thus portending potential systemic use for tumor treatment.

3.4. Systemic treatment of pancreatic tumors

Given that polyplex micelles of R-PEG20C appeared to retain potency for systemic application with enhanced blood circulation property and transfection ability, we attempted to test their therapeutic effect in the treatment of subcutaneous xenografts of pancreatic adenocarcinoma. The pancreatic cancer is one of the most intractable solid tumors [32], and it is worth noting that BxPC3 xenografts share the histopathologic characteristics of the human pancreatic adenocarcinoma: The xenografts have fibrotic parts, and tumor vasculature and nests of tumor cells embedded in the fibrotic parts [22,33]. It is also noteworthy in this model that all of 1) endothelial cells in tumor blood vessels, 2) fibroblast cells in tumor stroma and 3) tumor cells *per se* overexpress $\alpha_v\beta_3$ and $\alpha_v\beta_5$ integrin receptors, which are recognition motifs for the cRGD peptide, so all of these cells in the model can be the targets for cRGD micelles. On the other hand, the characteristic features of pancreatic tumor, as mentioned above as common characteristics in humans and BxPC3 xenografts, which are reduced vascular permeability due to pericyte coverage of tumor vessels and thick fibrosis, may be an obstacle to deliver massive amount of therapeutic gene to the whole pancreatic tumor cells. Regarding to this, we attempted to apply an antiangiogenic approach, aiming to suppress tumor growth through inhibition of neo-vasculature formation [34–36]. As a pDNA payload for a tumor gene therapy test, we selected a secreted protein, soluble sFlt-1, which exerts antiangiogenesis by trapping angiogenic molecules (VEGF) [37]. From the result of maximal cell transfection efficiency at N/P 8 (Fig. 1c), R-PEG20C prepared at N/P 8 was evaluated. As shown in Fig. 4b, PEG20C without a ligand molecule [cRGD(−)] (N/P 8) displayed an inhibitory effect on tumor growth compared with control groups, moreover R-PEG20C with ligand molecule [cRGD(+)] exerted a significantly more potent tumor suppression effect than PEG20C, supporting the strategy of ligand conjugation for promoting systemic antitumor efficacy.

To confirm that the observed antitumor efficacy was due to loaded sFlt-1 pDNA expression at the tumor site, we immunostained the lightly fixed cyro-section of tumor tissue with an antibody which binds to both membrane-bound Flt-1, or VEGF receptor 1 (VEGFR1), and sFlt-1/sVEGFR1. The expression of total VEGFR1/Flt-1 (green) was remarkably more in the mice

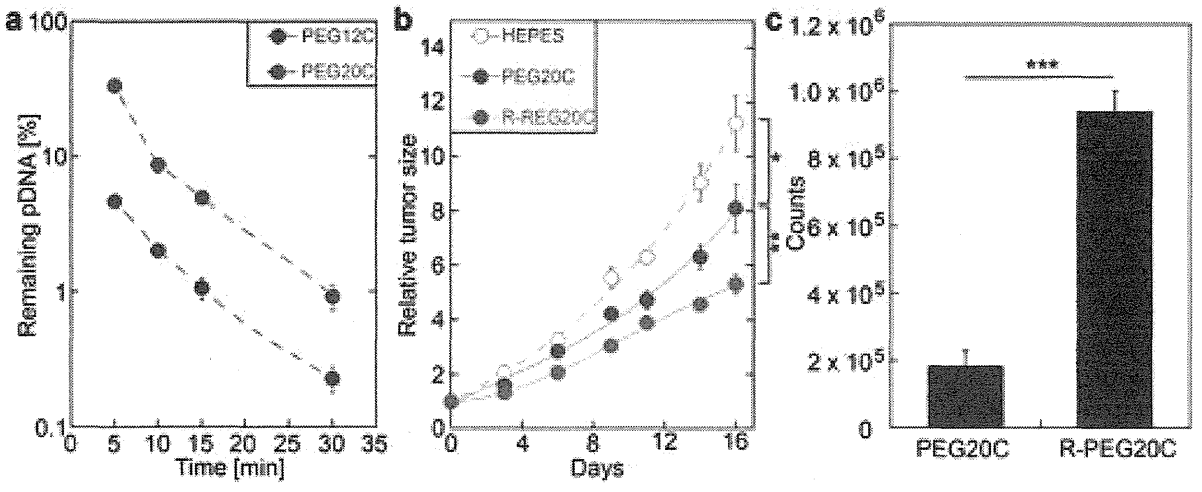

Fig. 4. *In vivo* evaluation after systemic administration of polyplex micelles. (a): PEG length effect on retention in the blood circulation determined by RT-PCR. (b): Antitumor activity in terms of tumor size (mean ± SEM, $n = 3$). The polyplex micelle was intravenously administered through the tail vein for three times on days 0, 4 and 8. Data points marked with asterisks are statistically significance of PEG20C vs HEPES and R-PEG20C vs PEG20C. (*$p < 0.05$ and **$p < 0.01$; Student's *t*-test). (c): Accumulations of polyplex micelles in the tumor 24 h after intravenous injection of polyplex micelles loading Cy5-labeled DNA into BxPC3-tumor bearing mice. The fluorescence intensity was expressed as photon counts normalized by tumor weight (***$p < 0.005$; Student's *t*-test).

administered with PEG20C and R-PEG20C as compared to the control sample (Fig. 5). In particular, R-PEG20C displayed higher gene expression than with PEG20C, concurrently in good agreement with inhibitory effect on tumor growth. Noteworthy, the location of the expressed sFlt-1 was found to be enriched in the tumor stroma adjacent to the vascular endothelial cells (red), rather than in the tumor nest (cell nucleus stained in blue). In view of the function of VEGF molecule to stimulate growth of and to maintain existence of neo-vasculature, it is reasonable that the expressed sFlt-1 secreted from the transfected cells may be found to localize there as a consequence of entrapping VEGF molecules. Furthermore, to investigate the benefits of the cRGD motif for targeted accumulation of polyplex micelles into the tumor site, polyplex micelles of PEG20C and R-PEG20C prepared from pDNA labeled with Cy5 fluorescent dye were intravenously administered into the bloodstream. The tumor accumulation of polyplex micelles was quantified by measurement of the fluorescence intensity of Cy5 in homogenized tumor tissue (Fig. 4c). Apparently, R-PEG20C exhibited markedly higher tumor accumulation, approximately five times higher than that of PEG20C. Finally, to confirm the antiangiogenic effect of loaded sFlt-1 gene expression from R-PEG20C, vascular endothelial cells were immunostained with PECAM-1. The quantified vascular density (Fig. 6) of tumors treated by R-PEG20C was significantly lower than that of the control sample ($^{**}p < 0.01$). Overall, these results confirmed that the accumulation of R-PEG20C into a targeted tumor site facilitated marked loaded antiangiogenic gene expression at the targeted tumor site, resulting in an antiangiogenic effect for inhibition on neo-vasculature growth and eventually suppressing tumor growth.

The investigations above approved that polyplex micelle with improved PEG shielding and ligand molecule conjugation led to active targeted accumulation into a tumor site, along with the promotion of cellular uptake and favorable intracellular trafficking, produced pronounced gene expression in the targeted cells and elicited a potent therapeutic effect for antitumor treatment through the antiangiogenic pathway. This result validates the feasibility of ligand molecule (cRGD peptide) conjugation with our proposed polyplex micelle having an improved blood retention profile for potential use in systemic targeted delivery to a desired site. It particularly provides important implications for versatile use in the treatment of diverse diseases by assigning approximate ligands onto the surface of the polyplex micelle for systemic gene therapy.

4. Conclusions

Aiming for developing gene delivery carrier for systemic use, promotion of PEG shielding and utilization of ligand molecules for tumor targeting was proposed on PEG-PAsp(DET) based polyplex micelles. Increased retention in blood circulation was successfully achieved by virtue of enhanced PEG shielding through conjugation

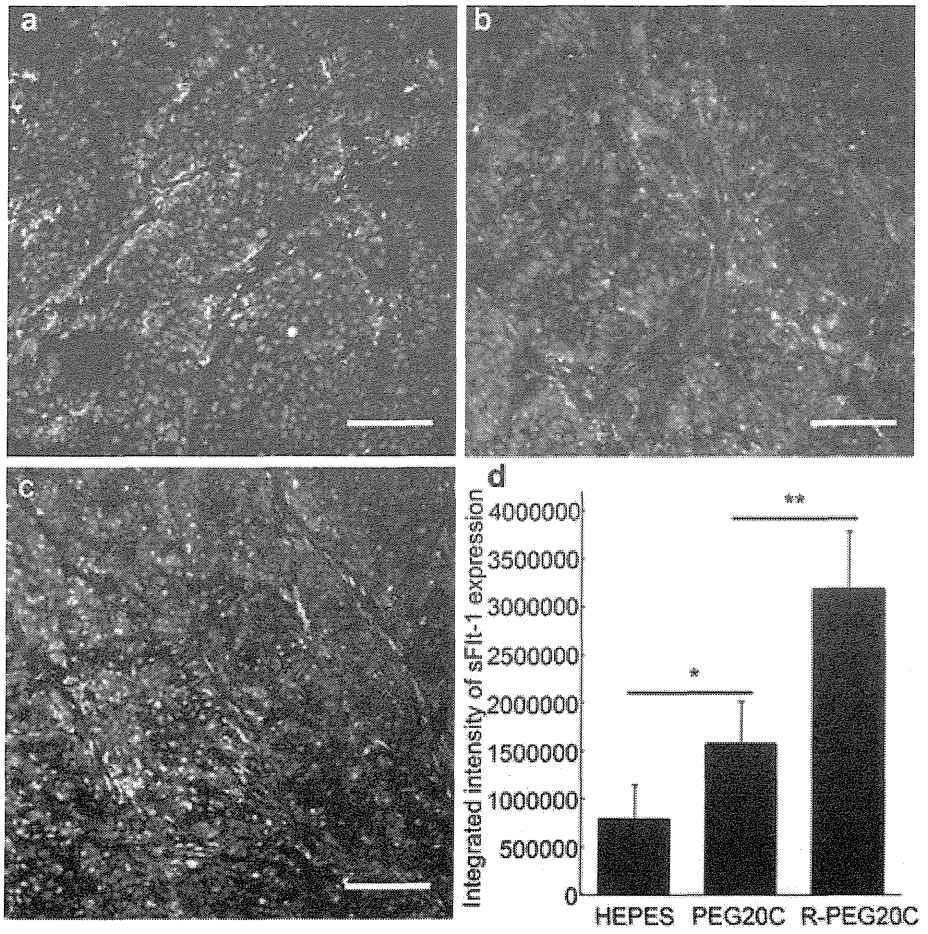

Fig. 5. Expression of sFlt-1 protein in tumor tissue after systemic injection of polyplex micelles. (a): HEPES buffer as a control; (b): PEG20C; and (c): R-PEG20C. Blue: nucleus; Red: vascular endothelial cells immunostained positive with PECAM1. Green: expressed sFlt-1 (or inherent VEGFR1). The scale bars represent 200 μm in all CLSM images. (d) Integral intensity of Flt-1/VEGFR1-positive region (green) were quantified from the images (mean ± SEM, $n = 4$; $^{*}p < 0.05$ and $^{**}p < 0.01$, Student's t-test).

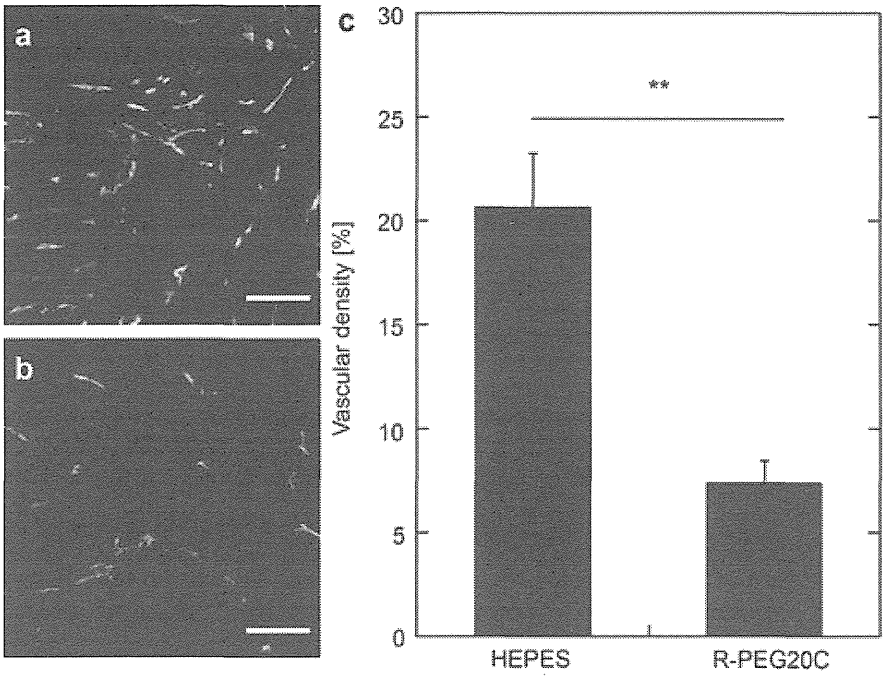

Fig. 6. Vasculature of sFlt-1 treated tumors observed by CLSM of immunostaining PECAM-1-positive-vascular endothelial cells in the BxPC3 tumor tissue. (a): HEPES and (b): R-PEG20C loading sFlt-1 pDNA. The scale bars represent 100 μm in all CLSM images. (c): Areas of PECAM-1-positive region (green) quantified from CLSM images (mean ± SEM, $n = 8$; $^{**}p < 0.01$, Student's t-test).

of a cholesteryl group and with the use of a longer PEG, 20 kDa. Noteworthy was the strategic use of cholesteryl conjugation for enhanced PEG shielding: it increased the number of tethering PEG chains and compacted the polyplex micelle core more, synergistically increasing PEG density. Further elongation of PEG from 12 kDa to 20 kDa induced PEG for further crowding, which may afford significant contribution in avoiding rapid blood clearance mode. Furthermore, ligand conjugation onto the polyplex micelle surface contributed to both improved accumulation at the tumor site and enhanced gene expression of antiangiogenic protein through facilitated cellular uptake and intracellular trafficking. The proposed polyplex micelle with these features ultimately demonstrated significant tumor growth suppression as a result of its antiangiogenic effect. The results validate the systemic usage of this system for tumor-targeted gene therapy, thus endows tremendous future perspective of developing the system for broad utilities by choosing appropriate therapeutic genes and targeting moieties.

Acknowledgments

This work was financially supported by the Core Research Program for Evolutional Science and Technology (CREST) and Precursory Research for Embryonic Science and Technology (PRESTO) from the Japan Science and Technology Corporation (JST), and by the Japan Society for the Promotion of Science (JSPS) through its Funding Program for World-Leading Innovative R&D on Science and Technology (FIRST Program) and Core to Core Program for A. Advanced Research Networks. Q. C. acknowledges a fellowship from Ministry of Education, Science, Sports and Culture, Japan (MEXT). The authors are grateful to Ms. Y. Li and Ms. K. Machitani for their intellectual contributions to the discussion.

Appendix A. Supplementary data

Supplementary data related to this article can be found online at http://dx.doi.org/10.1016/j.biomaterials.2013.12.086

References

[1] Moghimi SM, Hunter AC, Murray JC. Nanomedicine: current status and future prospects. FASEB J 2005;19:311–30.
[2] Wagner V, Dullaart A, Bock AK, Zweck A. The emerging nanomedicine landscape. Nat Biotech 2006;24:1211–7.
[3] Mitragotri S, Lahann J. Physical approaches to biomaterial design. Nat Mater 2009;8:15–23.
[4] Cabral H, Nishiyama N, Kataoka K. Supramolecular nanodevices: from design validation to theranostic nanomedicine. Acc Chem Res 2011;44:999–1008.
[5] Lee Y, Kataoka K. Delivery of nucleic acid drugs. Adv Polym Sci 2012;249:95–134.
[6] Osada K, Christie RJ, Kataoka K. Polymeric micelles from poly(ethylene glycol)-poly(amino acid) block copolymer for drug and gene delivery. J R Soc Interface 2009;6:S325–9.
[7] Kanayama N, Fukushima S, Nishiyama N, Itaka K, Jang WD, Miyata K, et al. A PEG-based biocompatible block catiomer with high buffering capacity for the construction of polyplex micelles showing efficient gene transfer toward primary cells. Chem Med Chem 2006;1:439–44.
[8] Miyata K, Oba M, Nakanishi M, Fukushima S, Yamasaki Y, Koyama H, et al. Polyplexes from poly(aspartamide) bearing 1,2-diaminoethane side chains induce pH-selective, endosomal membrane destabilization with amplified transfection and negligible cytotoxicity. J Am Chem Soc 2008;130:16287–94.
[9] Itaka K, Ishii T, Hasegawa Y, Kataoka K. Biodegradable polyamino acid-based polycations as safe and effective gene carrier minimizing cumulative toxicity. Biomaterials 2010;31:3707–14.
[10] Miyata K, Nishiyama N, Kataoka K. Rational design of smart supramolecular assemblies for gene delivery: chemical challenges in the creation of artificial viruses. Chem Soc Rev 2012;41:2562–74.
[11] Nomoto T, Matsumoto Y, Miyata K, Oba M, Fukushima S, Nishiyama N, et al. In situ quantitative monitoring of polyplexes and polyplex micelles in the blood circulation using intravital real-time confocal laser scanning microscopy. J Control Release 2011;151:104–9.
[12] Andrade JD, Hlady V, Jeon SI. Poly(ethylene glycol) and protein resistance: principles, problems and possibilities. Adv Chem Ser 1996;248:51–9.
[13] Osada K, Kataoka K. Drug and gene delivery based on supermolecular assembly of PEG-polypeptide hybrid block copolymers. Adv Polym Sci 2006;202:113–53.
[14] Gref R, Luck M, Quellec P, Marchand M, Dellacherie E, Harnisch S, et al. 'Stealth' corona-core nanoparticles surface modified by polyethylene glycol (PEG): influences of the corona-core (PEG chain length and surface density) and of the core composition on phagocytic uptake and plasma protein adsorption. Colloids Surf B 2000;18:301–13.
[15] Moghimi SM, Szebenib J. Stealth liposomes and long circulating nanoparticles: critical issues in pharmacokinetics, opsonization and protein-binding properties. Prog Lipid Res 2003;42:463–78.

[16] Oba M, Miyata K, Osada K, Christie RJ, Sanjoh M, Li W, et al. Polyplex micelles prepared from ω-cholesteryl PEG-polycation block copolymers for systemic gene delivery. Biomaterials 2011;32:652–63.
[17] Tockary TA, Osada K, Chen Q, Machitani K, Dirisala A, Uchida S, et al. Tethered PEG crowdedness determining shape and blood circulation profile of polyplex micelle gene carriers. Macromolecules 2013;46:6585–92.
[18] Mickler FM, Vachutinsky Y, Oba M, Miyata K, Nishiyama N, Kataoka K, et al. Effect of integrin targeting and PEG shielding on polyplex micelle internalization studied by live-cell imaging. J Control Release 2011;156:364–73.
[19] Hwang R, Varner JV. The role of integrins in tumor angiogenesis. Hematol Oncol Clin North Am 2004;18:991–1006.
[20] Brooks PC, Clark RAF, Cheresh DA. Requirement of vascular integrin $\alpha_v\beta_3$ for angiogenesis. Science 1994;264:569–71.
[21] Kim H, Ishi T, Zheng M, Watanabe S, Toh K, Matsumoto Y, et al. Multifunctional polyion complex micelle featuring enhanced stability, targetability, and endosome escapability for systemic siRNA delivery to subcutaneous model of lung cancer. Drug Deliv Transl Res 2013. http://dx.doi.org/10.1007/s13346-013-0175-6.
[22] Kano MR, Bae Y, Iwata C, Morishita Y, Yashiro M, Oka M, et al. Improvement of cancer-targeting therapy, using nanocarriers for intractable solid tumors by inhibition of TGF-β signaling. Proc Natl Acad Sci U S A 2007;104:3460–5.
[23] Chen Q, Osada K, Ishii T, Oba M, Uchida S, Tockary TA, et al. Homo-catiomer integration into PEGylated polyplex micelle from block-catiomer for systemic antiangiogenic gene therapy for fibrotic pancreatic tumors. Biomaterials 2012;33:4722–30.
[24] Oba M, Aoyagi K, Miyata K, Matsumoto Y, Itaka K, Nishiyama N, et al. Polyplex micelles with cyclic RGD peptide ligands and disulfide cross-links directing to the enhanced transfection via controlled intracellular trafficking. Mol Pharm 2008;5:1080–92.
[25] Osada K, Oshima H, Kobayashi D, Doi M, Enoki M, Yamasaki Y, et al. Quantized folding of plasmid DNA condensed with block catiomer into characteristic rod structures promoting transgene efficacy. J Am Chem Soc 2010;132:12343–8.
[26] Kenausis GL, Voros J, Elbert DL, Huang N, Hofer R, Ruiz-Taylor L, et al. Poly(L-lysine)-g-poly(ethylene glycol) layers on metal oxide surfaces: attachment mechanism and effects of polymer architecture on resistance to protein adsorption. J Phys Chem B 2000;104:3298–309.
[27] Kawaguchi S, Imai G, Suzuki J, Miyahara A, Kitano T, Ito K. Aqueous solution properties of oligo- and poly(ethylene oxide) by static light scattering and intrinsic viscosity. Polymer 1997;38:2885–91.
[28] Parkhouse RME, Askonas BA, Dourmashkin RR. Electron microscopy studies of mouse immunoglobulin. Immunology 1970;18:575–84.
[29] Wright AK, Thompson MR. Hydrodynamic structure of bovine serum albumin determined by transient electric birefringence. Biophys J 1975;15:137–41.
[30] Suck D, Oefner C, Kabsch W. Three dimension structure of bovine pancreatic DNase I at 2.5 resolution. Embo J 1984;3:2423–30.
[31] Zuckerman JE, Choi CHJ, Han H, Davis ME. Polycation-siRNA nanoparticles can disassemble at the kidney glomerular basement membrane. Proc Natl Acad Sci U S A 2012;109:3137–42.
[32] Zuckerman DS, Ryan DP. Adjuvant therapy for pancreatic cancer: a review. Cancer 2008;112:243–9.
[33] Cabral H, Matsumoto Y, Mizuno K, Chen Q, Murakami M, Kimura M, et al. Accumulation of sub-100nm polymeric micelles in poorly permeable tumours depends on size. Nat Nanotech 2011;12:815–23.
[34] Oba M, Vachutinsky Y, Miyata K, Kano MR, Ikeda S, Nishiyama N, et al. Antiangiogenic gene therapy of solid tumor by systemic injection of polyplex micelles loading plasmid DNA encoding soluble Flt-1. Mol Pharm 2010;7:501–9.
[35] Vachutinsky Y, Oba M, Miyata K, Hiki S, Kano MR, Nishiyama N, et al. Antiangiogenic gene therapy of experimental pancreatic tumor by sFlt-1 plasmid DNA carried by RGD-modified crosslinked polyplex micelles. J Control Release 2011;149:51–7.
[36] Carmeliet P, Jain RK. Angiogenesis in cancer and other diseases. Nature 2000;407:249–57.
[37] Yamaguchi S, Iwata K, Shibuya M. Soluble Flt-1 (Soluble VEGFR-1), a potent natural antiangiogenic molecule in mammals, is phylogenetically conserved in avians. Biochem Biophys Res Commun 2002;291:554–9.

Journal of Controlled Release 178 (2014) 18–24

Contents lists available at ScienceDirect

Journal of Controlled Release

journal homepage: www.elsevier.com/locate/jconrel

Systemic siRNA delivery to a spontaneous pancreatic tumor model in transgenic mice by PEGylated calcium phosphate hybrid micelles

Frederico Pittella [a,b], Horacio Cabral [b], Yoshinori Maeda [b], Peng Mi [c], Sumiyo Watanabe [a], Hiroyasu Takemoto [c], Hyun Jin Kim [d], Nobuhiro Nishiyama [c], Kanjiro Miyata [a,*], Kazunori Kataoka [a,b,d,e,**]

[a] Center for Disease Biology and Integrative Medicine, Graduate School of Medicine, The University of Tokyo, 7-3-1 Hongo, Bunkyo-ku, Tokyo 113-0033, Japan
[b] Department of Bioengineering, Graduate School of Engineering, The University of Tokyo, 7-3-1 Hongo, Bunkyo-ku, Tokyo 113-8656, Japan
[c] Polymer Chemistry Division, Chemical Resources Laboratory, Tokyo Institute of Technology, R1-11, 4259 Nagatsuta, Midori-ku, Yokohama 226-8503, Japan
[d] Department of Materials Engineering, Graduate School of Engineering, The University of Tokyo, 7-3-1 Hongo, Bunkyo-ku, Tokyo 113-8656, Japan
[e] Center for NanoBio Integration, The University of Tokyo, 7-3-1 Hongo, Bunkyo-ku, Tokyo 113-8656, Japan

ARTICLE INFO

Article history:
Received 3 August 2013
Accepted 7 January 2014
Available online 15 January 2014

Keywords:
siRNA delivery
Calcium phosphate
PEG
Charge-conversional polymer
Transgenic mice
Spontaneous pancreatic carcinoma

ABSTRACT

Efficient systems for delivery of small interfering RNA (siRNA) are required for clinical application of RNA interference (RNAi) in cancer therapy. Herein, we developed a safe and efficient nanocarrier comprising poly(ethylene glycol)-*block*-charge-conversional polymer (PEG-CCP)/calcium phosphate (CaP) hybrid micelles for systemic delivery of siRNA and studied their efficacy in spontaneous bioluminescent pancreatic tumors from transgenic mice. PEG-CCP was engineered to provide the siRNA-loaded hybrid micelles with enhanced colloidal stability and biocompatibility due to the PEG capsule and with endosome-disrupting functionality due to the acidic pH-responsive CCP segment where the polyanionic structure could be converted to polycationic structure at acidic pH through *cis*-aconitic amide cleavage. The resulting hybrid micelles were confirmed to have a diameter of <50 nm, with a narrow size distribution. Intravenously injected hybrid micelles significantly reduced the luciferase-based luminescent signal from the spontaneous pancreatic tumors in an siRNA sequence-specific manner. The gene silencing activity of the hybrid micelles correlated with their preferential tumor accumulation, as indicated by fluorescence imaging and histological analysis. Moreover, there were no significant changes in hematological parameters in mice treated with the hybrid micelles. These results demonstrate the great potential of the hybrid micelles as siRNA carriers for RNAi-based cancer therapy.

1. Introduction

Small interfering ribonucleic acid (siRNA) provides new perspectives for the treatment of various diseases. It functions by obstructing a specific cellular process by reducing protein production in a sequence-specific manner, a phenomenon termed RNA interference (RNAi) [1–4]. In particular, the use of RNAi-based therapy is expected to have potential for treatment of cancer because cancerous cells overexpress several specific genes, including oncogenes [5,6]. In the development of an RNAi-based cancer therapy, systemic administration of siRNA is essential for its effective accumulation in the wide range of internal tumor tissues. However, intravenous injection of naked siRNA molecules results in their rapid enzymatic degradation and subsequent clearance through the kidneys [7,8]. Therefore, efficient carriers are required to ensure successful delivery of siRNA to the therapeutic site of action [3,6,9].

Calcium phosphate (CaP)-based nanocarriers, a promising delivery system, has been widely developed for delivering nucleic acids to mammalian cells [10–14]. These are readily prepared by mixing aqueous ionic solutions for efficient encapsulation of nucleic acids. In this regard, we have previously prepared poly(ethylene glycol) (PEG)-coated CaP hybrid micelles by utilizing PEG-polyanion block copolymers [12,15–20]. In these block copolymers, the polyanion segment acts as a binding moiety with CaP nanoparticles, whereas the PEG segment forms a nonionic and hydrophilic outer layer for enhanced colloidal stability and biocompatibility (Fig. 1A). Furthermore, our recent studies successfully demonstrated functionalization of the polyanion segment for efficient endosomal escape of the siRNA payload [19–21]. An acidic pH-responsive anionic moiety, *cis*-aconitic amide (Aco), was introduced into the cationic side chain of the endosome-disrupting polyaspartamide derivative, poly{*N*′-[*N*-(2-aminoethyl)-2-aminoethyl] aspartamide} (PAsp(DET)) (Fig. 1B). The obtained PAsp(DET-Aco) bearing a net negative charge was found to be inactive for membrane disruption at extracellular neutral pH. However, on reversion to the parent polycation PAsp(DET) by cleavage of the Aco moiety at endosomal acidic pH, membrane disruptivity was activated [thus, termed charge-conversional polymer (CCP)] (Fig. 1C) [22]. Ultimately, the systemic administration of PEG-CCP/CaP hybrid micelles carrying

* Corresponding author. Tel.: +81 3 5841 1701; fax: +81 3 5841 7139.
** Correspondence to: K. Kataoka, Center for Disease Biology and Integrative Medicine, Graduate School of Medicine, The University of Tokyo, 7-3-1 Hongo, Bunkyo-ku, Tokyo 113-0033, Japan. Tel.: +81 3 5841 7138; fax: +81 3 5841 7139.
E-mail addresses: miyata@bmw.t.u-tokyo.ac.jp (K. Miyata), kataoka@bmw.t.u-tokyo.ac.jp (K. Kataoka).

0168-3659/$ – see front matter © 2014 Elsevier B.V. All rights reserved.
http://dx.doi.org/10.1016/j.jconrel.2014.01.008

vascular endothelial growth factor (VEGF) siRNA achieved significant antitumor activity in a murine xenograft model of subcutaneous pancreatic tumors [20]. These results demonstrated the great potential of this system for use as a cancer therapy and motivated us to investigate this system further.

To confirm the translational capability of promising nanocarriers, relevant preclinical tumor models, which parallel the microenvironment characteristics of tumors in the clinic, should be considered. In animal tumor models prepared by implantation of exogenous cancer cells or tissues, the tumoral microenvironment presents substantial differences with that of tumors in patients, including stroma, vasculature, lymphatics, immune cells, and increased population of certain clonal fractions due to selective stresses during cell culture or tissue transplantation [23,24]. These features in transplanted models are expected to affect the nanocarrier-mediated delivery of siRNA as well as drugs, *e.g.*, efficiencies of penetration, accumulation, and gene silencing in tumor tissues. In this regard, in genetically engineered tumor models, the tumor development closely relates to the clinical setting of the disease, with immune responses, angiogenesis, and inflammation naturally interrelating with the tumor [23]. Therefore, by using such spontaneous tumor models, siRNA-loaded nanocarriers could be evaluated in tumors with more relevant microenvironment and cell populations.

In the present study, we applied siRNA-loaded hybrid micelles in a genetically engineered pancreatic tumor model, in which the tumor gradually arises *in situ* and is associated with normal immune, angiogenesis, and inflammatory processes. The EL1-Luc/TAg transgenic mice used in this study spontaneously develop bioluminescent pancreatic adenocarcinoma owing to the SV40 T and firefly luciferase transgene constructs, which are regulated by the rat EL1 promoter [25]. SV40 T alters molecular, physiological, and histological aspects comparable to the tumorigenesis of acinar cell carcinoma in humans. Moreover, EL1-Luc/TAg transgenic mice permit non-invasive tracing of tumors through bioluminescence imaging because the cancer cells exclusively express luciferase. Accordingly, *in vivo* RNAi activity of the hybrid micelles carrying luciferase siRNA (siLuc) was determined by quantifying the luminescent signal from the pancreatic tumors after intravenous injection. To verify the validity of the measured RNAi activity, the tumor accumulation profile of the hybrid micelles was further assessed. To the best of our knowledge, this is the first study to demonstrate the effective delivery of siRNA to a spontaneous tumor model in transgenic mice by systemic administration.

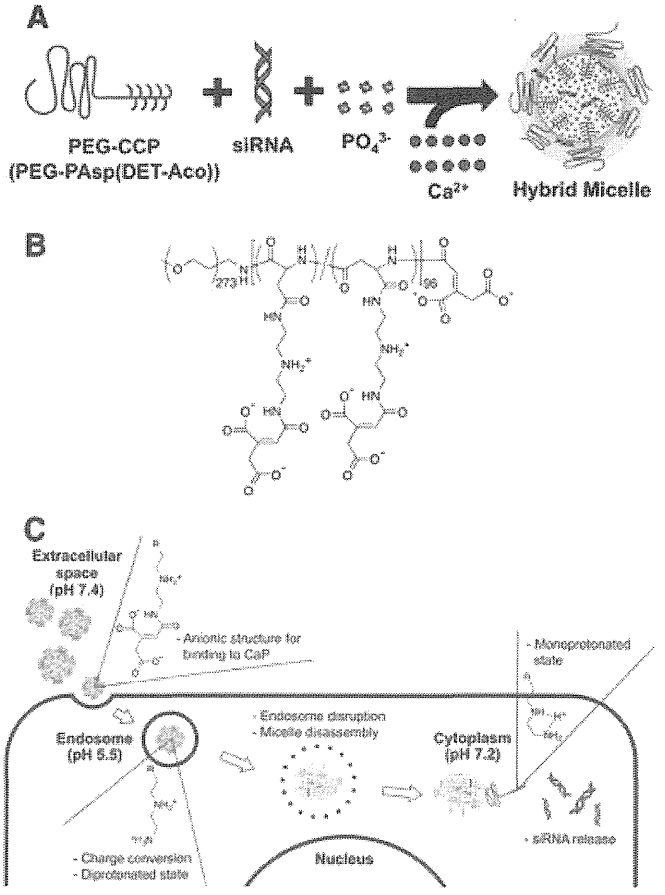

Fig. 1. (A) Schematic illustration of the preparation of hybrid micelles with PEG-CCP, siRNA, and CaP. (B) Chemical structure of PEG-PAsp(DET-Aco), termed PEG-CCP. (C) Schematic illustration of the cellular delivery of siRNA by PEG-CCP/CaP hybrid micelles. At extracellular neutral pH, PEG-CCP binds to the CaP nanoparticle, generating a PEG outer layer. Once endocytosed by the cell, the hybrid micelles undergo endosomal acidification. During acidification, PEG-CCP is converted to the parent PEG-PAsp(DET) through cleavage of the *cis*-aconitic amide bond, exposing the diprotonated side chain structure for endosomal membrane disruption. Finally, the siRNA payload is released into the cytoplasm, while the PAsp(DET) segment adopts the membrane-inactive monoprotonated side chain at cytoplasmic neutral pH.

2. Materials and methods

2.1. Materials, cell lines, and animals

$CaCl_2$ (anhydrous), Na_3PO_4, NaCl, HCl, ethanol, and phosphate buffered saline (PBS) were purchased from Wako Pure Chemical Industries Ltd. (Osaka, Japan). Dulbecco's modified Eagle's medium (DMEM) and penicillin/streptomycin stabilized solution were purchased from Sigma-Aldrich (St. Louis, MO). *In vivo* grade luciferin VivoGlo, cell culture lysis buffer, and the Luciferase Assay System were purchased from Promega Corporation (Madison, WI). Tissue-Tek OCT compound and fetal bovine serum (FBS) were acquired from Sakura Finetek USA, Inc. (Torrance, CA) and Dainippon Sumitomo Pharma Co., Ltd. (Osaka, Japan), respectively. Methoxy-poly(ethylene glycol)-*block*-poly(*N*″-{*N*′-[(*N*-*cis*-aconityl)-2-aminoethyl]-2-aminoethyl}aspartamide) (PEG-PAsp(DET-Aco) or PEG-CCP) was synthesized as previously described, and then characterized by ^{1}H NMR (PEG: 12 kDa; PAsp(DET-Aco): 34 kDa) [19,20]. Firefly luciferase siRNA (siLuc) and its control siRNA (siScr) were synthesized by Hokkaido System Science (Hokkaido, Japan). The sequences of the siLuc were: 5′-CUU ACG CUG AGU ACU UCG AdTdT-3′ (sense) and 5′-UCG AAG UAC UCA GCG UAA GdTdT-3′ (antisense); the sequences of the siScr were: 5′-UUC UCC GAA CGU GUC ACG UdTdT-3′ (sense) and 5′-ACG UGA CAC GUU CGG AGA AdTdT-3′ (antisense). Fluorescently labeled siLuc was obtained by introducing Alexa Fluor 647 to the 5′ end of sense strand from GeneDesign, Inc. (Osaka, Japan).

HeLa-Luc, a firefly luciferase-expressing human cervical cancer cell line, was purchased from Caliper Life Science (Hopkinton, MA). The cells were maintained in DMEM containing 10% FBS and 1% streptomycin/penicillin in a humidified atmosphere containing 5% CO_2 at 37 °C. FVB/NJc1 female mice (18–20 g, 6 weeks) were purchased from Clea Japan, Inc. (Tokyo, Japan). EL1-Luc/EL1-SV40 T-antigen transgenic mice (OncoMouse; male, 18–20 g, 6 weeks) were purchased from Caliper Life Sciences (Hopkinton, MA). Female FVB mice and male transgenic mice were allowed to breed, and the newborn mice were genotyped primarily by basal bioluminescence imaging at the age of 5 weeks. Male mice presenting basal luminescence in the pancreas were separated for use in the experiments. All animal experiments were performed in accordance with the Guidelines for the Care and Use of Laboratory Animals as stated by The University of Tokyo.

2.2. Preparation of hybrid micelles

Hybrid micelles were prepared as previously described [20]. In brief, a solution of 2.5 M $CaCl_2$ (1 μL) was diluted in 10 mM Tris buffer (pH 10) (11.5 μL). Another solution containing PEG-CCP (1.0 mg/mL) in 10 mM Tris/HCl buffer (pH 7.5) was mixed with a solution of 15 μM siRNA in 10 mM HEPES buffer (pH 7.2) and with 50 mM HEPES buffer containing 1.5

mM Na_3PO_4 and 140 mM NaCl (pH 7.5) (2.5 μL:5 μL:5 μL). The former solution was mixed with the latter solution by pipetting up and down for approximately 20 s (final siRNA concentration: 3 μM). The freshly prepared micelle solution containing 40 μg siRNA and 100 μg PEG-CCP (1 mL) was then purified and concentrated using a VivaSpin-06 device (molecular weight cut-off (MWCO): 10 kDa). The ultrafiltration was performed in a swing bucket rotor at 900 *g* and 4 °C for 20 min. To minimize non-specific binding of micelles to the membrane, the centrifuge filter devices were washed with de-ionized water before use. After centrifugation, the retained solution (100 μL) was added to 300 mM NaCl solution (100 μL) to adjust the final concentration to 150 mM NaCl. Through this procedure, the excess free calcium ions were removed from the micelle solution to the flow-through. The quantity of calcium removed was determined using a calcium sensitive dye, arsenazo III, by the SRL Laboratories (SRL Inc., Tokyo, Japan).

2.3. Transmission electron microscopic (TEM) imaging

Hybrid micelle solution (20 μL) was loaded on a 400-mesh copper grid and stained with 20 μL of uranyl acetate solution (2%, w/v) for 5 s. The copper grids with carbon-coated collodion film were glow-discharged for 10 s with an Eiko IB-3 ion coater (Eiko Engineering Co. Ltd., Japan) prior to use. The morphology of hybrid micelles was observed on a JEM-1400 (JEOL Ltd., Tokyo, Japan) with 100 kV acceleration voltage and 40 μA beam current, toward high resolution and high contrast with high performance imaging of specimens.

2.4. In vitro luciferase gene silencing

HeLa-Luc cells were seeded in a 96-well plate at a cell density of 2500 cells/well in 0.1 mL of DMEM containing 10% FBS and then precultured for 24 h. Before transfection, the medium was refreshed. Hybrid micelles containing siRNA (siLuc or siScr), hybrid micelles without siRNA (mock), or naked siRNA (siLuc or siScr) were applied to each well to final siRNA concentrations of 100 and 200 nM (n = 6). After 48 h of incubation, the medium was removed and the cells were washed twice with 100 μL of PBS. The cells were then lysed with 50 μL of cell culture lysis buffer. The luciferase expression in the lysate was determined from photoluminescence intensity using the Luciferase Assay System and Mithras LB 940 (Berthold Technologies). The relative luciferase activity was calculated as a ratio to that in non-treated cells.

2.5. Biodistribution and tumor accumulation of hybrid micelles in transgenic mice

Mice were fed with alfalfa-free food *ad libitum*. A group of three male transgenic mice (15 weeks) were intravenously injected with Alexa Fluor 647-labeled siLuc (Alexa647-siLuc) contained in hybrid micelles (200 μL, 20 μg siRNA). As a control, the same amount of naked Alexa647-siLuc was also injected to another group of male transgenic mice. Intravenous injection was performed slowly (10 s per injection) to avoid adverse side effects. Mice were sacrificed 6 h after the injection, and then the main organs (heart, lungs, liver, spleen, kidneys, and pancreas, including tumors) were excised for fluorescent imaging using IVIS (Caliper Life Sciences, Hopkinton, MA). Organs were washed in PBS and kept on ice prior to analysis. Similarly, blood was collected from mice at 6 h after the injection, and then it was centrifuged at 2000 *g* for 10 min to obtain the plasma. The fluorescence intensity was determined using the Living Image software through the selection of an ROI around the whole organ/tumor and the plasma, and then it was converted to the % of dose/g of tissue (or plasma) based on a standard curve. To avoid incomplete separation of tumors from the pancreas, the combined weight of the organ and tumors was used for the subsequent statistical data analysis.

2.6. Tumor histology

After the biodistribution studies described in the preceding section were complete, a portion of the pancreas/tumor tissue from each mouse was rapidly frozen in Tissue-Tek OCT compound with liquid nitrogen in ethanol. The frozen pancreas/tumor tissues embedded in the block were then cut into 6-μm thick slices at −20 °C with a Tissue-Tek Cryo3 microtome/cryostat (Sakura Finetek USA, Inc., Torrance, CA). Each section of the pancreas/tumor tissue was fixed with formalin and stained with hematoxylin and eosin (HE) for histological identification of tumor cells and healthy pancreatic cells. In addition to HE staining, adjacent cryosections of the pancreas/tumor tissue were stained with Hoechst 33342 (Dojindo Lab., Kumamoto, Japan) for observation of cellular nuclei using a confocal laser scanning microscope (CLSM) (LSM 510, Carl Zeiss, Germany). The CLSM observation was performed at the excitation wavelengths of 633 nm (He–Ne laser) and 710 nm (MaiTai laser, two photon excitation) for Alexa647-siRNA and Hoechst 33342, respectively. The fluorescence intensities of the Alexa647-siRNA from the tumor region or the healthy pancreatic region in the obtained CLSM image were determined using the ImageJ software.

2.7. In vivo luminescence reduction in transgenic mice

Hybrid micelle solutions containing 20 μg of siLuc or siScr (200 μL) were slowly injected into the caudal vein of transgenic mice (13 weeks; n = 16). Bioluminescence intensity in the pancreatic tumors was determined before injection and 24 h after injection of the hybrid micelles using an IVIS instrument. Mice were anesthetized with isoflurane and luciferin was injected intraperitoneally at a dosage of 150 mg/kg (200 μL). Measurements were performed 10 min after luciferin injection for three different positions in each mouse (right flank, left flank, and ventral positions) to reduce variability in bioluminescence due to the tumor positions. Photons emitted from the pancreas region were quantified using the Living Image software and summed from the 3 positions. All images were set to the same conditions and color scale.

2.8. Hematological parameters and cytokine levels

Hybrid micelle solutions containing 20 μg of siScr (200 μL) were slowly injected in the caudal vein of female Balb/c mice (6 weeks). Blood was collected at several time points after the injection and centrifuged at 2000 *g* for 10 min to obtain the plasma. The levels of alkaline phosphatase (ALP), aspartate aminotransferase (AST), alanine aminotransferase (ALT), and creatinine (Cr) in the plasma were measured by the SRL Laboratories (SRL Inc., Tokyo, Japan) (n = 5). Also, the levels of tumor necrosis factor-α (TNF-α), interleukin-6 (IL-6), IL-1α, and IL-1β in plasma were determined by Quantikine® ELISA kits, according to the manufacturer's protocol (n = 4).

3. Results and discussion

3.1. Preparation of hybrid micelles

Preparation of CaP nanoparticles in an aqueous solution is known to result in the formation of insoluble large aggregates over time. Thus, PEG-CCP (Fig. 1B) was used to prepare CaP nanoparticles with enhanced colloidal stability through the steric repulsive effect of the PEG capsule. These nanoparticles also had endosome-disrupting functionality derived from the CCP segment. This segment was synthesized through the introduction of an Aco moiety into the side chain of PAsp(DET) through *cis*-aconitic amide bond formation. Successful preparation of PEG-CCP (or quantitative introduction of the Aco moiety) was confirmed using ^{1}H NMR spectroscopy (data not shown), as previously described [19]. The resulting PAsp(DET-Aco) segment was stable at neutral pH, whereas under acidic conditions, it underwent *cis*-aconitic amide cleavage to revert back to the parent PAsp(DET) (Fig. 1C) [22].

The generated PAsp(DET) enabled acidic pH-selective membrane disruption based on the distinctive change in the protonation state of the side chain unit, *i.e.*, the monoprotonated state at neutral pH and the diprotonated state at acidic pH, directed toward endosomal escape of the payload (Fig. 1C) [26,27].

The hybrid micelles were prepared by simple mixing of a solution containing PEG-CCP, siRNA, and phosphate ions, with a solution of calcium ions (Fig. 1A). The prepared micelles were then subjected to ultrafiltration (MWCO: 10 kDa) for the removal of excess free calcium ions as well as for concentration of the sample. The concentrated solution was diluted with the same volume of NaCl solution (300 mM) to generate the hybrid micelle solution at 150 mM NaCl. The obtained hybrid micelles were observed with a high performance TEM. Fig. 2A depicts spherical nanoparticles of approximately 30 nm in diameter with a clearly narrow size distribution, which was confirmed by the size distribution histogram obtained from analyses of the TEM images (mean diameter: 33.2 nm, n = 111) (Fig. 2B). The hybrid micelle solution was further characterized by dynamic light scattering (DLS) and electrophoretic light scattering. The size of hybrid micelles was 38 nm at the peak of the number-weighted histogram in DLS (Supporting Fig. S1), associated with a narrow size distribution (polydispersity index = 0.09). This size is consistent with that estimated from the TEM images. Further, the zeta-potential of hybrid micelles was almost neutral (−2.2 mV), consistent with the presence of nonionic PEG outer layer. In addition, the DLS analysis revealed that the cumulant size of the hybrid micelles was maintained over 7 days of storage at 4 °C (data not shown), demonstrating the potential for long-term storage in a refrigerator.

3.2. In vitro luciferase gene silencing

To confirm *in vitro* siRNA delivery efficacy, the hybrid micelles carrying siLuc were applied to a luciferase assay with cultured HeLa-Luc cells as a luciferase-expressing model cell line. After 48 h of incubation, siLuc delivered by the hybrid micelles significantly decreased the luciferase expression in a dose-dependent manner (Fig. 3); the hybrid micelles inhibited approximately 50% and 90% of luciferase expression at 100 nM and 200 nM siRNA, respectively. In sharp contrast, the hybrid micelles with a control sequence of siRNA (siScr) as well as the mock micelles without siRNA resulted in no reduction in luciferase expression, indicating sequence-specific, potent gene silencing ability of the hybrid micelles. In our previous studies, the hybrid micelles exhibited a significant gene silencing effect on endogenous VEGF in cultured pancreatic cancer cells (PanC-1 and BxPC3) [19,20], suggesting that their gene silencing ability is not limited to a specific target gene and cell line. The efficient gene silencing ability of the hybrid micelles was probably due to the stable encapsulation of siRNA in CaP nanoparticles in cell culture medium [20], followed by efficient cellular internalization and endosomal escape induced by the CCP segment [19]. With regard to the cellular internalization, our previous study revealed that hybrid micelles were efficiently uptaken by HeLa cells within 4 h, probably due to an energy-dependent endocytosis [16]. It should be noted that no significant cytotoxicity was observed for any of the samples at the tested concentrations, as determined in a cell viability assay using a water soluble tetrazolium salt (WST-8) (data not shown).

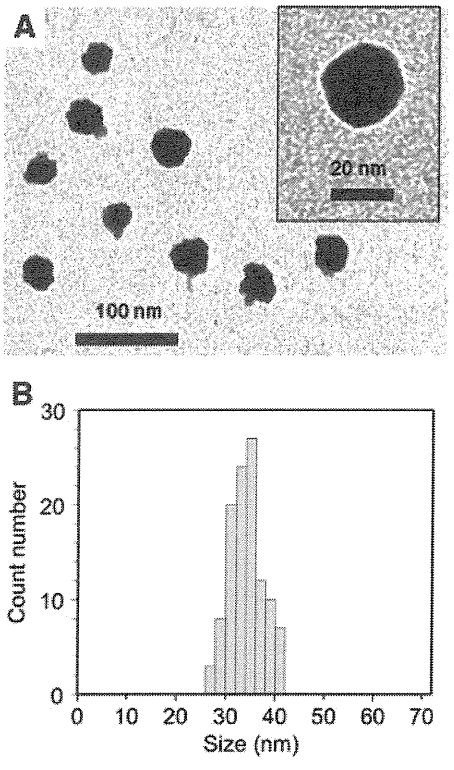

Fig. 2. (A) TEM image of the hybrid micelles. (B) Size distribution histogram of the hybrid micelles based on their TEM images.

3.3. Biodistribution and tumor accumulation of hybrid micelles in transgenic mice

Biodistribution of hybrid micelles after intravenous injection was evaluated in the transgenic mice presenting spontaneous pancreatic tumors using Alexa647-siRNA. At 6 h after injection, the transgenic mice were sacrificed, and the organs were excised for measuring fluorescence intensity, which was then converted to the % of dose/g of tissue based on a standard curve. As the border between a pancreatic tumor and healthy pancreas tissue is unclear, the fluorescence intensity of the whole pancreatic tissue was measured for tumor accumulation of Alexa647-siRNA. Note that the significant fluorescence was not detected from the collected blood samples, indicating that almost all the hybrid micelles (or Alexa647-siRNAs) were eliminated from the bloodstream within 6 h. Thus, the fluorescence intensity measured from each organ would not be affected by blood circulating micelles. As shown in Fig. 4, the amount of hybrid micelles was approximately 0.9% of dose/g of pancreas/tumor, which was 6-fold larger than that in naked siRNA. No significant difference between hybrid micelles and naked siRNA was observed for the accumulation in other organs; however, the kidneys displayed lower accumulation for Alexa647-siRNA delivered by the hybrid micelles compared to naked siRNA. These results suggest that the hybrid micelles could protect Alexa647-siRNA from rapid renal filtration, enabling it to circulate for longer in the blood, and therefore accumulate more in the pancreas/tumor.

The enhanced accumulation of hybrid micelles in the pancreas/tumor was further investigated by histological analysis. First, HE-stained sections were prepared to facilitate distinction of the tumor region (T) from healthy pancreatic tissue (H). As depicted in Fig. 5A, healthy pancreatic cells were organized into lobules toward formation of glandular acini. In contrast, tumor cells show a non-organized solid growth pattern [28,29]. Fig. 5A also shows the presence of connective tissue septa in between the T and H areas. CLSM was then performed to image the corresponding Hoechst 33342-stained sections. It is noteworthy that fluorescence signals from Alexa647-siRNA delivered by hybrid micelles were found mainly in the tumor region (Fig. 5B). Quantitative analysis using the ImageJ software indicated that the fluorescence signal of Alexa647-siRNA in the tumor region was 2.9-fold stronger than that in the healthy pancreas. By considering that the average weight of pancreas/tumor in the transgenic mice was 2.2-fold higher than that of pancreas in wild-type mice, the tumor accumulation of siRNA delivered by hybrid micelles can be roughly estimated to be ~1.3% of dose/g of tumor with the assumption that the tissue weights are similar between tumor and healthy pancreas in the transgenic mice. Thus, the

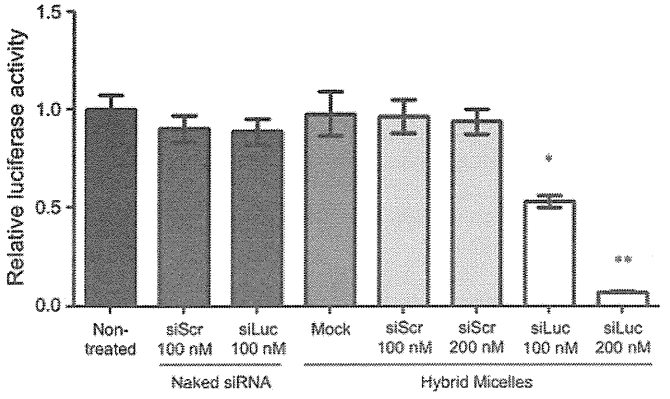

Fig. 3. *In vitro* luciferase gene silencing by hybrid micelles in cultured HeLa-Luc cells. Luciferase luminescence was quantified after 48 h of incubation of cells treated with samples. Results are expressed as mean and standard deviation (n = 6). $^{*}P < 0.05$; $^{**}P < 0.001$ (ANOVA followed by Newman–Keuls).

preferential tumor accumulation of siRNA-loaded hybrid micelles was demonstrated in the spontaneous pancreatic tumor model.

In a previous study, we reported that the tumor vasculature in the EL1-Luc/TAg transgenic mice was covered with pericytes [30], which can considerably limit the penetration of nanocarriers into the spontaneous tumor model in comparison to hypervascular and/or less stromal tumor models [31,32]. Nevertheless, the hybrid micelles apparently penetrated and distributed within the tumors (Fig. 5B). This behavior should be attributed to the relatively small size of the hybrid micelles (approximately 30–40 nm in diameter, Fig. 2 and Supporting Fig. S1), facilitating the passage of the nanocarriers through the tumor vasculature and stromal tissues. This was in agreement with our recent study where <50-nm polymeric micelles efficiently penetrated into the tissue, even in hypopermeable tumor models, which was in contrast to the control micelles that were >50 nm in size [33]. It should be further noted that the enhanced tumor accumulation behavior of hybrid micelles, compared to naked siRNA, in the present spontaneous pancreatic tumors was comparable to our previous observation in a subcutaneous BxPC3 tumor model [20]. This can also be explained by the small size of hybrid micelles, as the small-sized nanocarriers may be less affected by the tumor microenvironments restricting extravasation and penetration of nanocarriers, such as pericyte coverage of the vasculature [33]. Altogether, the hybrid micelles are a promising strategy for the systemic delivery of siRNA to various and whole tumor tissues/cells.

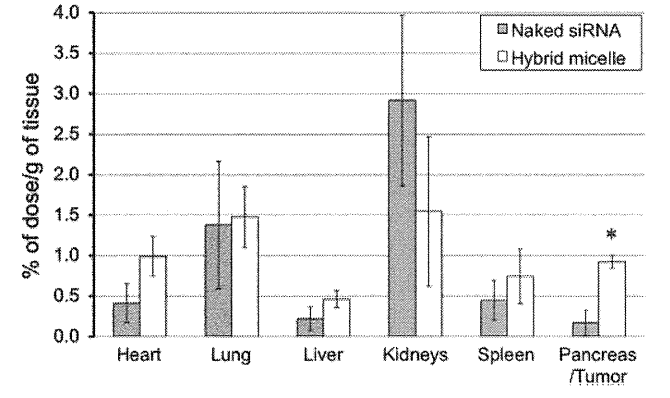

Fig. 4. Biodistribution of Alexa647-siRNA-loaded hybrid micelles and naked Alexa647-siRNA by fluorescence quantification at 6 h after intravenous injection (20 μg siRNA/injection) in 14-week-old transgenic mice. The obtained fluorescence intensities were converted to % of dose/g of tissue based on a standard curve. Results are expressed as mean and standard error of mean (n = 3). ANOVA followed by Newman–Keuls ($^{*}P < 0.01$).

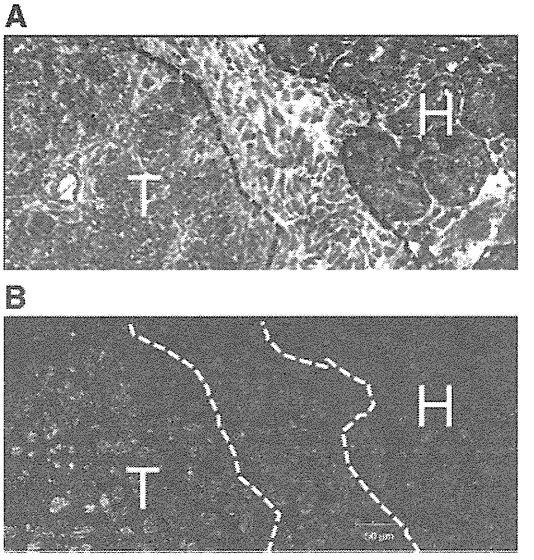

Fig. 5. Histological observation of pancreas/tumor in transgenic mice treated with hybrid micelles. Sections were prepared from the pancreas/tumor tissue excised at 6 h after intravenous injection of hybrid micelles carrying Alexa647-siRNA (20 μg siRNA/injection) to transgenic mice. (A) HE staining: non-organized tumor cells (T) and healthy pancreatic structure in lobes (H) are separated by the dotted line. (B) CLSM image of an adjacent section to that stained with HE. Nuclei (blue) were stained with Hoechst 33342, and Alexa647-siRNA is shown in green. (For interpretation of the references to color in this figure legend, the reader is referred to the web version of this article.)

3.4. In vivo luciferase gene silencing in transgenic mice

Pancreatic cancer is considered to be one of the most fatal cancers [34]. Moreover, the all-stage 5-year survival has not improved greatly during the last 25 years [35]. These facts have motivated us to develop novel therapeutics to improve the prognosis of pancreatic cancer patients. An immunocompetent mouse presenting spontaneous pancreatic tumors is a useful model for establishment of such novel therapeutics, including anticancer drug-loaded micelles [30]. Herein, the *in vivo* gene silencing activity of hybrid micelles was evaluated with the spontaneous pancreatic tumor model developed in EL1-Luc/TAg transgenic mice, in which the expression of firefly luciferase is promoted specifically in the acinar cell carcinoma [25]. Accordingly, this model can be used for a gene silencing assay that employs the bioluminescence of the pancreatic tumors. It is worth noting that the following characteristics were confirmed for the spontaneous pancreatic cancer model in the previous study [30]; i) liver and intestine metastases are likely to occur in this model after the mice becoming 16 weeks old, ii) the pancreas/tumor in this model is enlarged and also the pancreatic cancer may grow over the normal position of pancreas, and iii) the bioluminescent signal from the pancreatic cancer is not always emitted from the same anatomic position. Considering these points, the bioluminescence measurements in this study were performed for 3 different positions, *i.e.*, left flank, frontal, and right flank of the 13-week-old mice without detectable tumor metastases.

Representative bioluminescence images of the left flank position of mice treated with or without siLuc-loaded hybrid micelles are shown in Fig. 6A, where the variable bioluminescence signals from the pancreatic tumor can be identified. At 24 h after systemic injection of the hybrid micelles, the bioluminescence intensity in the pancreatic tumors exhibited a significant reduction of 61% compared with the initial intensity before injection (Fig. 6B; $P < 0.01$), indicating that the hybrid micelles induced efficient luciferase gene silencing in the tumor tissue. There was no significant reduction in the bioluminescence signal after injection of siScr-loaded hybrid micelles, indicating that the reduction in the bioluminescence intensity was due to the sequence-specific

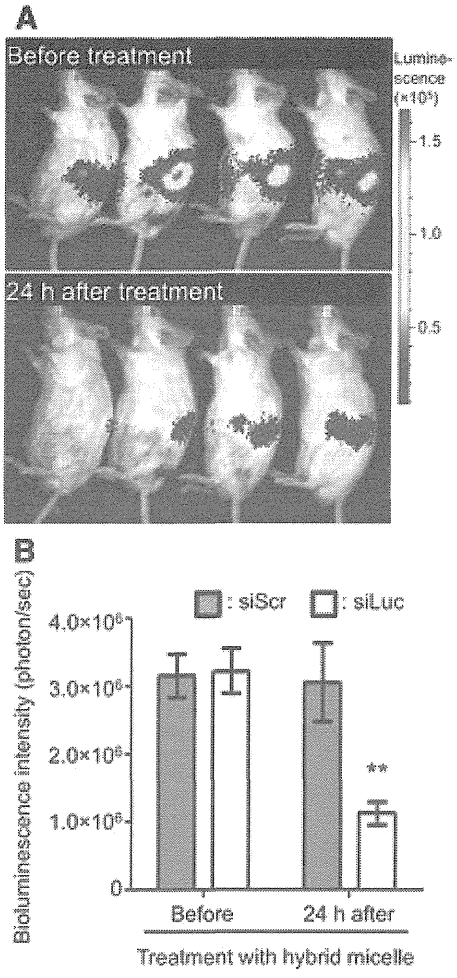

Fig. 6. *In vivo* gene silencing activity of systemically administered hybrid micelles in the spontaneous pancreatic tumors of transgenic mice. (A) Representative images of mice before and 24 h after injection of hybrid micelles containing siLuc (20 μg siRNA/mouse). (B) Bioluminescence intensity in the pancreatic tumors after intravenous injection of hybrid micelles containing siLuc or siScr (20 μg siRNA/mouse). Results are expressed as mean and standard deviation (n = 16). ANOVA followed by Newman–Keuls (**$P < 0.01$).

RNAi machinery. The similar gene silencing profile of hybrid micelles was further observed for the protein amount of luciferase in homogenized pancreas/tumor tissues (Supporting Fig. S2). This sequence-specific gene silencing activity of hybrid micelles is consistent with their significantly enhanced tumor accumulation of the siRNA payload (Figs. 4 and 5), which was roughly estimated to be ~1.3% of dose/g of tumor, corresponding to ~40 ng siRNA. Interestingly, the *in vivo* gene silencing efficacy of hybrid micelles in the spontaneous pancreatic cancer cells (60% with ~40 ng siRNA) was apparently higher than the *in vitro* efficacy in the cultured HeLa-Luc cells (50% with ~130 ng siRNA). These different efficacies might be due to varying cellular innate functions between the *in vivo* pancreatic cancer cells and the *in vitro* monolayer-cultured cervical cancer cells. The cellular innate functions, including the expression levels of luciferase and RNAi-related genes, are known to be substantially altered between live tissue and cell culture, especially monolayer culture, and also different types of cells [36–38]. Indeed, the luciferase expression in the present pancreatic cancer cells was lost in monolayer culture. This is the reason for the use of HeLa-Luc cells as a conventional cancer cell line for demonstrating the *in vitro* gene silencing activity of hybrid micelles.

3.5. Hematological parameters and cytokine levels after systemic administration of hybrid micelles

To verify the safety of the hybrid micelle formulation, hematological parameters and inflammatory cytokine levels were measured at several time points after systemic administration. As summarized in Table 1, the intravenous injection of hybrid micelles induced no remarkable changes in the levels of AST, ALT, and ALP as indicators of liver function and that of Cr as an indicator of kidney function over 48 h, suggesting negligible adverse side effects on the liver and the kidneys. Similarly, the levels of inflammatory cytokines, *i.e.*, TNF-α, IL-6, IL-1α, and IL-1β, were not affected by the injection of hybrid micelles (Supporting Fig. S3). Overall, it was demonstrated that the intravenous injection of hybrid micelles induced no severe acute toxicity under the tested conditions.

4. Conclusion

In the present study, hybrid micelles prepared with a smart block copolymer PEG-CCP were applied for systemic siRNA delivery to spontaneous pancreatic tumors in EL1-Luc/TAg transgenic mice. The obtained results confirmed the enhanced accumulation of siRNA-loaded hybrid micelles in the tumor tissue and their significant gene silencing activity. Notably, this was associated with negligible changes in hematological parameters. Altogether, the great potential of the hybrid micelles for RNAi-based cancer therapy was successfully demonstrated.

Acknowledgment

This research was funded by the Japan Society for the Promotion of Science (JSPS) through the "Funding Program for World-Leading Innovative R&D on Science and Technology (FIRST Program)," the Adaptable and Seamless Technology Transfer Program through Target-driven R&D (A-STEP), the National Institute of Biomedical Innovation (NIBIO), and Grants-in-Aid for Scientific Research from the Japanese Ministry of Health, Labour and Welfare. Part of this work was conducted in the Research Hub for Advanced Nano Characterization, The University of Tokyo, supported by the Ministry of Education, Culture, Sports, Science and Technology (MEXT), Japan. The authors are grateful to S. Ogura and K. Date for their assistance with animal care.

Appendix A. Supplementary data

Supplementary data to this article can be found online at http://dx.doi.org/10.1016/j.jconrel.2014.01.008.

References

[1] A. Fire, S. Xu, M.K. Montgomery, S.A. Kostas, S.E. Driver, C.C. Mello, Potent and specific genetic interference by double-stranded RNA in *Caenorhabditis elegans*, Nature 391 (1998) 806–811.

Table 1
Hematological parameters after intravenous injection of hybrid micelles (20 μg siRNA/mouse).

	Non-treated (0 min)	10 min	30 min	60 min	120 min	20 h	48 h
AST (U/L)	40 ± 5	38 ± 9	42 ± 4	40 ± 5	41 ± 5	36 ± 4	47 ± 7
ALT (U/L)	61 ± 18	62 ± 13	73 ± 5	67 ± 8	64 ± 12	86 ± 28	61 ± 23
ALP (U/L)	401 ± 25	401 ± 22	424 ± 10	378 ± 8	384 ± 23	377 ± 28	477 ± 37
Cr (mg/dL)	0.11 ± 0.01	0.11 ± 0.01	0.11 ± 0.01	0.10 ± 0.01	0.10 ± 0.01	0.10 ± 0.02	0.07 ± 0.01

Abbreviations: AST, aspartate aminotransferase; ALT, alanine aminotransferase; ALP, alkaline phosphatase; Cr, creatinine. Results are expressed as mean and standard deviation (n = 5).

[2] S.M. Elbashir, J. Harborth, W. Lendeckel, A. Yalcin, K. Weber, T. Tuschl, Duplexes of 21-nucleotide RNAs mediate RNA interference in cultured mammalian cells, Nature 411 (2001) 494–498.
[3] K. Whitehead, R. Langer, D. Anderson, Knocking down barriers: advances in siRNA delivery, Nat. Rev. Drug Discov. 8 (2009) 129–138.
[4] J.C. Burnett, J.J. Rossi, RNA-based therapeutics: current progress and future prospects, Chem. Biol. 19 (2012) 60–71.
[5] F. Takeshita, T. Ochiya, Therapeutic potential of RNA interference against cancer, Cancer Sci. 97 (2006) 689–696.
[6] Y.-K. Oh, T.G. Park, siRNA delivery systems for cancer treatment, Adv. Drug Deliv. Rev. 61 (2009) 850–862.
[7] F. van de Water, O. Boerman, A. Wouterse, J. Peters, F. Russel, R. Masereeuw, Intravenously administered short interfering RNA accumulates in the kidney and selectively suppresses gene function in renal proximal tubules, Drug Metab. Dispos. 34 (2006) 1393–1397.
[8] J. Turner, S. Jones, S. Moschos, M. Lindsay, M. Gait, MALDI-TOF mass spectral analysis of siRNA degradation in serum confirms an RNase A-like activity, Mol. Biosyst. 3 (2007) 43–50.
[9] R.J. Christie, N. Nishiyama, K. Kataoka, Delivering the code: polyplex carriers for deoxyribonucleic acid and ribonucleic acid interference therapies, Endocrinology 151 (2010) 466–473.
[10] C.A. Chen, H. Okayama, Calcium phosphate-mediated gene-transfer—a highly efficient transfection system for stably transforming cells with plasmid DNA, Biotechniques 6 (1988) 632.
[11] M. Jordan, A. Schallhorn, F.M. Wurm, Transfecting mammalian cells: optimization of critical parameters affecting calcium-phosphate precipitate formation, Nucleic Acids Res. 24 (1996) 596–601.
[12] Y. Kakizawa, K. Kataoka, Block copolymer self-assembly into monodispersive nanoparticles with hybrid core of antisense DNA and calcium phosphate, Langmuir 18 (2002) 4539–4543.
[13] M. Zhang, K. Kataoka, Nano-structured composites based on calcium phosphate for cellular delivery of therapeutic and diagnostic agents, Nano Today 4 (2009) 508–517.
[14] J. Li, Y.C. Chen, Y.C. Tseng, S. Mozumdar, L. Huang, Biodegradable calcium phosphate nanoparticle with lipid coating for systemic siRNA delivery, J. Control. Release 142 (2010) 416–421.
[15] Y. Kakizawa, K. Miyata, S. Furukawa, K. Kataoka, Size-controlled formation of a calcium phosphate-based organic–inorganic hybrid vector for gene delivery using poly(ethylene glycol)-block-poly(aspartic acid), Adv. Mater. 16 (2004) 699–702.
[16] Y. Kakizawa, S. Furukawa, K. Kataoka, Block copolymer-coated calcium phosphate nanoparticles sensing intracellular environment for oligodeoxynucleotide and siRNA delivery, J. Control. Release 97 (2004) 345–356.
[17] Y. Kakizawa, S. Furukawa, A. Ishii, K. Kataoka, Organic–inorganic hybrid-nanocarrier of siRNA constructing through the self-assembly of calcium phosphate and PEG-based block aniomer, J. Control. Release 111 (2006) 368–370.
[18] M. Zhang, A. Ishii, N. Nishiyama, S. Matsumoto, T. Ishii, Y. Yamasaki, K. Kataoka, PEGylated calcium phosphate nanocomposites as smart environment-sensitive carriers for siRNA delivery, Adv. Mater. 21 (2009) 3520–3525.
[19] F. Pittella, M. Zhang, Y. Lee, H.J. Kim, T. Tockary, K. Osada, T. Ishii, K. Miyata, N. Nishiyama, K. Kataoka, Enhanced endosomal escape of siRNA-incorporating hybrid nanoparticles from calcium phosphate and PEG-block charge-conversional polymer for efficient gene knockdown with negligible cytotoxicity, Biomaterials 32 (2011) 3106–3114.
[20] F. Pittella, K. Miyata, Y. Maeda, T. Suma, Q. Chen, R.J. Christie, K. Osada, N. Nishiyama, K. Kataoka, Pancreatic cancer therapy by systemic administration of VEGF siRNA contained in calcium phosphate/charge-conversional polymer hybrid nanoparticles, J. Control. Release 161 (2012) 868–874.
[21] H. Takemoto, K. Miyata, S. Hattori, T. Ishii, T. Suma, S. Uchida, N. Nishiyama, K. Kataoka, Acidic pH-responsive siRNA conjugate for reversible carrier stability and accelerated endosomal escape with reduced IFNα-associated immune response, Angew. Chem. Int. Ed. 52 (2013) 6218–6221.
[22] Y. Lee, K. Miyata, M. Oba, T. Ishii, S. Fukushima, M. Han, H. Koyama, N. Nishiyama, K. Kataoka, Charge conversion ternary polyplex with endosomes disruption moiety: a technique for efficient and safe gene delivery, Angew. Chem. Int. Ed. 120 (2008) 5241–5244.
[23] K.K. Frese, D.A. Tuveson, Maximizing mouse cancer models, Nat. Rev. Cancer 7 (2007) 654–658.
[24] G. Francia, W. Cruz-Munoz, S. Man, P. Xu, R.S. Kerbe, Mouse models of advanced spontaneous metastasis for experimental therapeutics, Nat. Rev. Cancer 11 (2011) 135–141.
[25] N. Zhang, S. Lyons, E. Lim, P. Lassota, A spontaneous acinar cell carcinoma model for monitoring progression of pancreatic lesions and response to treatment through noninvasive bioluminescence imaging, Clin. Cancer Res. 15 (2009) 4915–4924.
[26] K. Miyata, M. Oba, M. Nakanishi, S. Fukushima, Y. Yamasaki, H. Koyama, N. Nishiyama, K. Kataoka, Polyplexes from poly(aspartamide) bearing 1,2-diaminoethane side chains induce pH-selective, endosomal membrane destabilization with amplified transfection and negligible cytotoxicity, J. Am. Chem. Soc. 130 (2008) 16287–16294.
[27] K. Miyata, N. Nishiyama, K. Kataoka, Rational design of smart supramolecular assemblies for gene delivery: chemical challenges in the creation of artificial viruses, Chem. Soc. Rev. 41 (2012) 2562–2574.
[28] L.A. Aaltonen, S.R. Hamilton, World Health Organization; international agency for research on cancer, in: L.A. Aaltonen, S.R. Hamilton (Eds.), Pathology and Genetics of Tumours of the Digestive System, IARC Press: Oxford University Press, Lyon: Oxford, 2000, (314 pp.).
[29] R.A. Caruso, A. Inferrera, G. Tuccari, G. Barresi, Acinar cell carcinoma of the pancreas, a histologic, immunocytochemical and ultrastructural study, Histol. Histopathol. 9 (1994) 53–58.
[30] H. Cabral, M. Murakami, H. Hojo, Y. Terada, M.R. Kano, U.-I. Chung, N. Nishiyama, K. Kataoka, Targeted therapy of spontaneous murine pancreatic tumors by polymeric micelles prolongs survival and prevents peritoneal metastasis, Proc. Natl. Acad. Sci. U. S. A. 110 (2013) 11397–11402.
[31] M.R. Kano, Y. Bae, C. Iwata, Y. Morishita, M. Yashiro, M. Oka, T. Fujii, A. Komuro, K. Kiyono, M. Kaminishi, K. Hirakawa, Y. Ouchi, N. Nishiyama, K. Kataoka, K. Miyazono, Improvement of cancer-targeting therapy, using nanocarriers for intractable solid tumors by inhibition of TGF-β signaling, Proc. Natl. Acad. Sci. U. S. A. 104 (2007) 3460–3465.
[32] L. Zhang, H. Nishihara, M.R. Kano, Pericyte-coverage of human tumor vasculature and nanoparticle permeability, Biol. Pharm. Bull. 35 (2012) 761–766.
[33] H. Cabral, Y. Matsumoto, K. Mizuno, Q. Chen, M. Murakami, M. Kimura, Y. Terada, M.R. Kano, K. Miyazono, M. Uesaka, N. Nishiyama, K. Kataoka, Accumulation of sub-100 nm polymeric micelles in poorly permeable tumours depends on size, Nat. Nanotechnol. 6 (2011) 815–823.
[34] American Cancer Society, Cancer Facts & Figs. 2011, Epidemiologic Surveillance Report, American Cancer Society, Atlanta, 2011, (available at: <http://www.cancer.org/acs/groups/content/@epidemiologysurveilance/documents/document/acspc-029771.pdf>. Accessed April 2013).
[35] A. Jemal, R. Siegel, J. Xu, E. Ward, Cancer statistics, 2010, CA Cancer J. Clin. 260 (2010) 277–300.
[36] F. Pampaloni, E.G. Reynaud, E.H.K. Stelzer, The third dimension bridges the gap between cell culture and live tissue, Nat. Rev. Mol. Cell Biol. 8 (2007) 839–845.
[37] N.J. Yoo, S.Y. Hur, M.S. Kim, J.Y. Lee, S.H. Lee, Immunohistochemical analysis of RNA-induced silencing complex-related proteins AGO2 and TNRC6A in prostate and esophageal cancers, APMIS 118 (2010) 271–276.
[38] T. Endo, K. Itaka, M. Shioyama, S. Uchida, K. Kataoka, Gene transfection to spheroid culture system on micropatterned culture plate by polyplex nanomicelle: a novel platform of genetically-modified cell transplantation, Drug Deliv. Transl. Res. 2 (2012) 398–405.

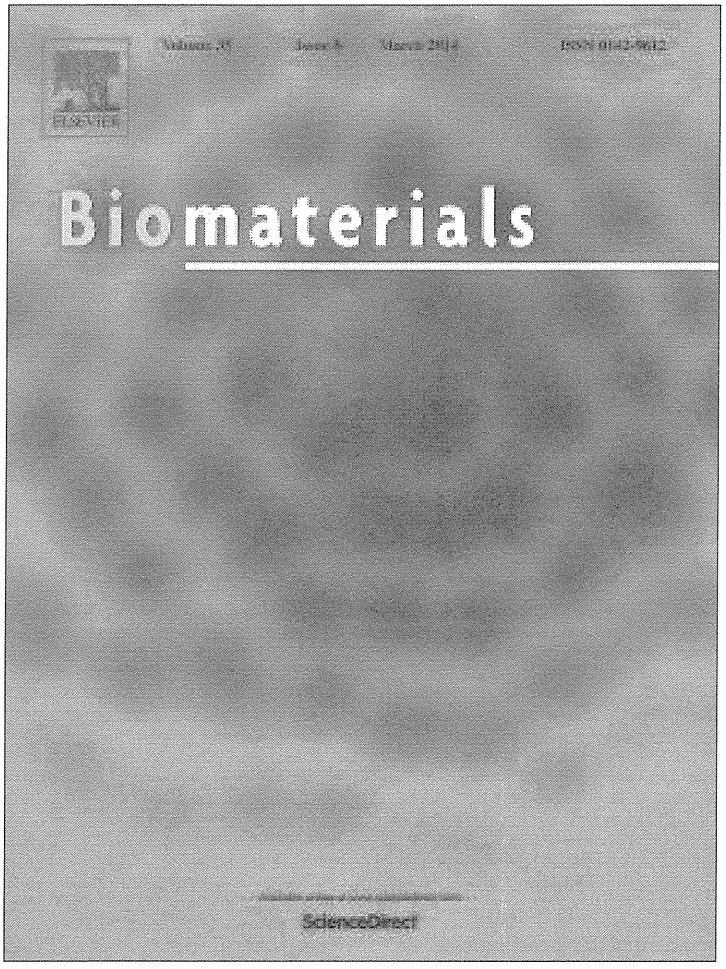

Biomaterials 35 (2014) 2499–2506

Contents lists available at ScienceDirect

Biomaterials

journal homepage: www.elsevier.com/locate/biomaterials

An injectable spheroid system with genetic modification for cell transplantation therapy

Satoshi Uchida [a], Keiji Itaka [a,*], Takahiro Nomoto [b], Taisuke Endo [c], Yu Matsumoto [d], Takehiko Ishii [b], Kazunori Kataoka [a,b,c,**]

[a] Division of Clinical Biotechnology, Center for Disease Biology and Integrative Medicine, Graduate School of Medicine, The University of Tokyo, 7-3-1 Hongo, Bunkyo-ku, Tokyo 113-0033, Japan
[b] Department of Bioengineering, Graduate School of Engineering, The University of Tokyo, Tokyo, Japan
[c] Department of Materials Engineering, Graduate School of Engineering, The University of Tokyo, 7-3-1 Hongo, Bunkyo-ku, Tokyo 113-8656, Japan
[d] Department of Otorhinolaryngology and Head and Neck Surgery, Graduate School of Medicine and Faculty of Medicine, The University of Tokyo, Tokyo, Japan

ARTICLE INFO

Article history:
Received 13 November 2013
Accepted 8 December 2013
Available online 31 December 2013

Keywords:
Spheroid
Cell transplantation
Gene transfection
Nanomicelle
Non-viral carrier

ABSTRACT

The new methodology to increase a therapeutic potential of cell transplantation was developed here by the use of three-dimensional spheroids of transplanting cells subsequent to the genetic modification with non-viral DNA vectors, polyplex nanomicelles. Particularly, spheroids in regulated size of 100-μm of primary hepatocytes transfected with luciferase gene were formed on the micropatterned culture plates coated with thermosensitive polymer, and were recovered in the form of injectable liquid suspension simply by cooling the plates. After subcutaneously transplanting these hepatocyte spheroids, efficient transgene expression was observed in host tissue for more than a month, whereas transplantation of a single-cell suspension from a monolayer culture resulted in an only transient expression. The spheroid system contributed to the preservation of innate functions of transplanted hepatocytes in the host tissue, such as albumin expression, thereby possessing high potential for expressing transgene. Intravital observation of transplanted cells showed that those from spheroid cultures had a tendency to localize in the vicinity of blood vessels, making a favorable microenvironment for preserving cell functionality. Furthermore, spheroids transfected with erythropoietin-expressing DNA showed a significantly higher hematopoietic effect than that of cell suspensions from monolayer cultures, demonstrating high potential of this genetically-modified spheroid transplantation system for therapeutic applications.

1. Introduction

Cell transplantation therapy has attracted considerable attention for the treatment of various intractable diseases. The therapeutic potential of cell transplantation is primarily dependent on the efficacy and longevity of bioactive factors secreted from the transplanted cells [1]. In this respect, genetic modification of transplanted cells by introducing transgene(s) using either viral or non-viral methods is a promising approach to modulate the secretion of bioactive factors [2]. In addition to endogenous factors, transgenes expressing functional proteins and peptides such as growth factors and coagulation factors can further enhance the therapeutic potential of transplanted cells [3–5]. Furthermore, a scheme to maintain transplanted cells in optimal long-acting conditions is a key for successful treatment. Although the survival rate of cells varies depending on cell type and source, therapeutic effects are likely to be limited by the death of transplanted cells or the loss of cell activity due to unfavorable microenvironments such as ischemia, hypoxia, or inflammation [6].

Three-dimensional (3D) spheroid cell culture is a promising technique to improve cell survival and function by preserving cell-to-cell interactions. Several groups including ours have reported that 3D spheroid cultures could increase the survival rate of the cells and enhance innate functions such as albumin secretion from primary hepatocytes and multilineage differentiation of mesenchymal stem cells (MSCs) [7–12]. Recently, we introduced a procedure in genetically-modified cell transplantation using a 3D spheroid culture system on micropatterned culture plates (Cell-

* Corresponding author. Tel.: +81 3 5841 1418; fax: +81 3 5841 1419.
** Corresponding author. Division of Clinical Biotechnology, Center for Disease Biology and Integrative Medicine, Graduate School of Medicine, The University of Tokyo, 7-3-1 Hongo,Bunkyo-ku, Tokyo 113-0033, Japan Tel.: +81 3 5841 7138; fax: +81 3 5841 7139.
E-mail addresses: itaka-ort@umin.net (K. Itaka), kataoka@bmw.t.u-tokyo.ac.jp (K. Kataoka).

0142-9612/$ – see front matter © 2013 Elsevier Ltd. All rights reserved.
http://dx.doi.org/10.1016/j.biomaterials.2013.12.012

able™ multi-well plates; Transparent, Chiba, Japan) combined with gene transfection by polyplex nanomicelles [13]. The polyplex nanomicelle is a non-viral gene carrier composed of plasmid DNA (pDNA) and poly(ethylene glycol) (PEG)–polycation block copolymers, which possesses core–shell structure consisting of PEG shell and inner core of pDNA in a condensed state [14–16]. For the polycation, we developed poly[*N*′-[*N*-(2-aminoethyl)-2-aminoethyl] aspartamide] [PAsp(DET)]. This polycation possesses two distinguished properties: the efficient capability of endosomal escape and rapid biodegradability in the cytoplasm, allowing safe and effective gene introduction into various cells [17–19]. Using this polyplex nanomicelle system, we achieved high and prolonged transgene expression for more than one month from the spheroids of rat primary hepatocytes cultured on micropatterned plates [13]. The nanomicelle-treated spheroids also exhibited sustained albumin secretion at a level comparable with that exhibited by untreated spheroids, suggesting that this system allows safe gene transfection without impairing the innate function of hepatocytes.

In this study, the hepatocyte spheroids gene-transfected by the polyplex nanomicelles were transplanted into mice to obtain insight into their application in cell therapy. For transplanting spheroids in their intact 3D form, we introduced thermosensitive property to the micropatterned culture plate, which allows the recovery of spheroids simply by lowering the temperature of the plate. Then, hepatocyte spheroids transfected with luciferase expressing pDNA were transplanted to subcutaneous tissue to evaluate the efficiency of transgene expression in host animal. The advantages of this system were analyzed in detail by intravital imaging of transplanted cells in the host tissue. Finally, to examine therapeutic potential, hepatocyte spheroids receiving transfection with erythropoietin-expressing pDNA were transplanted, followed by evaluation of the hematopoietic effect in the host mice.

2. Materials & methods

2.1. Materials

Collagenase, dimethylsulfoxide (DMSO), dexamethasone, insulin, and L-proline nicotinamide were purchased from Wako Pure Chemical Industries (Osaka, Japan). Hank's buffered salt and L-ascorbic acid 2-phosphate (Asc-2P) were purchased from Sigma–Aldrich (St. Louis, MO, USA). Dulbecco's modified Eagle's medium (DMEM), trypsin inhibitor, and Pen-Strep-Glut (PSQ) were purchased from GIBCO (Frederich, MD, USA). Human epidermal growth factor (hEGF) was purchased from Toyobo (Osaka, Japan). Fetal bovine serum (FBS) was purchased from Dainippon Sumitomo Pharma (Osaka, Japan). For the construction of plasmid DNA (pDNA) expressing luciferase, the protein-expressing segment of pGL4.13 plasmid (Promega, Madison, WI, USA) was cloned into pCAG-GS plasmid (RIKEN, Tokyo, Japan) to obtain expression under CAG promoter/enhancer. For pDNA expressing Gaussia luciferase (Gluc), the protein-expressing segment of pCMV-Gluc control plasmid (New England BioLabs, Ipswich, MA, USA) was cloned into pCAG-GS. For pDNA expressing mouse erythropoietin (mEpo), protein expressing segments of pCMV-X4 plasmid (OriGene, Rockville, MD, USA) were cloned into pCAG-GS. These pDNAs were amplified in competent DH5α *Escherichia coli* and purified using a NucleoBond® Xtra Maxi Plus (Takara Bio, Shiga, Japan).

2.2. Animals

Balb/c nude mice (female; 7 weeks old) and Wistar rats (male; 5 weeks old) were purchased from Charles River Laboratories (Yokohama, Japan). Transgenic Sprague–Dawley (SD) rats (male; 5 weeks old) expressing EGFP in all tissues under the control of CAG promoter/enhancer (EGFP–SD rats) were purchased from Japan SLC (Shizuoka, Japan). All animal studies were conducted with the approval of the Animal Care and Use Committee of the University of Tokyo, Tokyo, Japan.

2.3. Isolation and culture of primary hepatocytes

Rat hepatocytes were isolated using a modified two-step collagenase digestion process as previously reported [20,21]. In brief, after the rat liver was perfused from the hepatic portal vein with a special solution described below, the collagenase solution was recirculated through the liver to obtain hepatocytes. The perfusion medium (pH 7.2) was composed of 8 g/L sodium chloride (NaCl), 400 mg/L potassium chloride (KCl), 78 mg/L sodium dihydrogen phosphate dehydrate ($NaH2PO4{\cdot}2H_2O$), 151 mg/L disodium hydrogen phosphate 12-water ($Na_2HPO_4{\cdot}12H_2O$), 2.38 g/L 2-[4-(2-hydroxyethyl)-1-piperazinyl] ethanesulfonic acid (HEPES), 190 mg/L ethylene glycol tetraacetic acid (EGTA), 350 mg/L sodium hydrogencarbonate ($NaHCO_3$), and 900 mg/L glucose. The collagenase solution (pH 7.2) was composed of 500 mg/L collagenase, 9.8 g/L Hank's buffered salt, 2.38 g/ml HEPES, 556 mg/ml calcium chloride hydrate ($CaCl_2{\cdot}H_2O$), 350 mg/L $NaHCO_3$, and 50 mg/L trypsin inhibitor. To preserve the function of hepatocytes under *in vitro* conditions, a special medium comprising DMEM supplemented with 10% FBS, 1% PSQ, 1% DMSO, 10^{-7} mol/L dexamethasone, 0.5 μg/ml insulin, 10 mmol/L nicotinamide, 0.2 mmol/L Asc-2P, and 10 ng/ml hEGF was used for cell culture [22].

2.4. Recovery and transplantation of the cells from spheroid and monolayer cultures

The micropatterned architecture was constructed on thermosensitive cell culture plates (Upcell™, CellSeed Inc., Tokyo, Japan) to prepare the thermosensitive micropatterned plates, in which cell adhesion sites of a 100-μm diameter are regularly arrayed surrounded by a non-adhesive area. Primary hepatocytes were seeded onto 12- or 96-well culture plates at densities of 4×10^5 cells/well or 4×10^4 cells/well, respectively. The spheroid cells were recovered as a suspension for transplantation studies by lowering the temperature without any damage to the structure of the spheroids. Cells on monolayer culture plates were recovered by trypsinization followed by centrifugation at 200× g for 3 min. The recovered suspension from a spheroid and monolayer culture was transplanted to the subcutaneous tissue of Balb/c nude mice by injection using 23-gauge needles. The number of cells to be transplanted per mouse was adjusted at the stage of seeding the cells onto the plate, to be 2×10^5, 4×10^5, and 1.2×10^6 for the transplantation to forelimb, abdomen, and earlobe, respectively. Because the number of recovered cells per well in 12-well plate was determined to be $(4.2 \pm 0.6) \times 10^5$, and $(4.8 \pm 0.7) \times 10^5$ (means ± SD) in spheroid and monolayer culture respectively, the number of transplanted cells per mouse were comparable between these two groups.

2.5. Gene introduction using polyplex nanomicelles

PEG–PAsp(DET) block copolymer and PAsp(DET) homopolymer were synthesized as previously reported [17]. PEG used in this study had a molecular weight (Mw) of 12,000, and the polymerization degree of the PAsp(DET) segment was determined to be 59 by ^{1}H-NMR. The polymerization degree of the PAsp(DET) homopolymer determined by ^{1}H-NMR was 55.

Polyplex nanomicelles were prepared as described in our previous report [13]. In brief, the nanomicelle was formed by mixing polymer and pDNA solutions in 10 mM Hepes buffer (pH 7.3). For preparing the polymer solution, we recently revealed that the combined use of two polymers, PEG–PAsp(DET) block copolymer and PAsp(DET) homopolymer, was advantageous to achieve both effective PEG shielding and functioning of PAsp(DET) to enhance endosomal escape [23]. Thus, in this study, nanomicelles were prepared by mixing pDNA solution with a premixed solution of the two polymers at the equal molar ratio of residual amino groups at the N/P ratio (residual molar ratio of total amino groups in the two polymers to phosphate groups in pDNA) of 10. The diameter of the resulting nanomicelles was determined to be approximately 70 nm by dynamic light scattering (DLS) [24]. In 12-well plate, a total of 10 μg of pDNA was added to 1 ml of culture medium for each well, and in 96-well plate, 1 μg of pDNA was added to 100 μl of culture medium.

2.6. In vivo and in vitro measurement of luciferase expression

In vivo luciferase expression after transplantation was measured using an IVIS™ Imaging System (Xenogen Corp., Alameda, CA, USA) after intravenous injection of D-luciferin (150 mg/kg, Sumisho Pharmaceuticals International, Tokyo, Japan).

In vitro analyses were performed using Gluc-expressing pDNA. Expressed Gluc is secreted into the culture medium and remains stable for more than a week [25]. In this study, to trace the real-time activity of transgene expression, the culture medium was replaced with fresh medium precisely 24 h before each indicated measuring point. 24 h after the replacement, the culture medium was collected to quantify Gluc secretion during the last 24 h, using a Renilla Luciferase Assay System (Promega) and GloMax® 96 Microplate Luminometer (Promega) following the manufacturer's protocol.

2.7. Quantification of transplanted cells and transgene and gene expression in host tissue

At 24 h after hepatocyte transplantation into the forelimb of mice, total DNA and mRNA in whole of the cutaneous and subcutaneous tissue in the forelimb were extracted from the transplantation site using DNeasy Blood & Tissue Kits (Qiagen, Hilden, Germany) and RNeasy Mini Kits (Qiagen), respectively, according to the manufacture's protocol. Using an ABI Prism 7500 Sequence Detector (Applied Biosystems, Foster City, CA, USA), quantitative real-time PCR (qRT-PCR) was performed. Because hepatocytes from male rats were transplanted to female mice, the number of transplanted cells in the host tissue was proportional to the copy number of SRY genes on Y chromosomes, which was amplified using the following primer pair: forward, CATCGAAGGGTTAAAGTGCCA; reverse, ATAGTGTGTAGGTTGTTGTCC, with standardization by quantifying pDNA copies of mouse β-actin (Mm00607939, Applied Biosystems). The number of transgenes (luciferase-expressing pDNA) in the host tissue was quantified using the following primer pair: forward,

TGCAAAAGATCCTCAACGTG; reverse, AATGGGAAGTCACGAAGGTG. The mRNA level of albumin expression was quantified and standardized with the mRNA level of β-actin using TaqMan® Gene Expression Assays (albumin: Rn00592480_m1, β-actin: Mm00607939, Applied Biosystems).

2.8. Intravital microscopic imaging of transplanted cells

The hepatocytes were isolated from EGFP–SD rats, and cultured as described above. The distribution of the cells was evaluated 24 h after transplantation to mouse earlobes using intravital real-time confocal laser scanning microscopy [26]. One hour before imaging, Evans Blue dye (2.5 mg/kg; Wako), which binds to serum albumin, was intravenously injected to visualize blood vessels. All picture acquisitions were performed using a Nikon A1R confocal laser scanning microscope system attached to an upright ECLIPSE FN1 microscope equipped with a Plan Apo λ 20X NA 0.75 objective lens (Nikon, Tokyo, Japan). The pinhole diameter was set to result in a 10-μm optical slice. For fluorescent imaging of EGFP and Evans Blue, 488 nm and 640 nm excitation lasers and band-pass emission filters of 525/50, and 700/75 nm was used, respectively. Acquired data were further processed using Nikon NIS Elements software.

3. Results

3.1. Transgene expression in host mice after transplantation of genetically-modified hepatocytes

Uniform spheroids from rat primary hepatocytes with a 100-μm diameter were prepared using micropatterned culture plates, in which cell adhesion areas of 100-μm diameter are regularly arrayed in a two-dimensional manner surrounded by non-adhesive areas coated by PEG matrix (Cell-able™ multi-well plate; Transparent, Chiba, Japan) [7]. The cell adhesion areas were coated with a polymer, poly(*N*-isopropylacrylamide) (PIPAAm), which is widely used in the temperature-responsive cell recovery system (Fig. 1a) [27–29]. After placing the plate on ice followed by the addition of cold phosphate-buffered saline (PBS), PIPAAm becomes hydrophilic, resulting in the detachment of spheroid from culture plates simply by pipetting. Thus, spheroids with uniform size of 100 μm were recovered in the form of an injectable suspension without disrupting their 3D structure (Fig. 1b).

The recovered spheroids were subcutaneously transplanted to mouse abdomen simply by injection with 23-gauge needles. It is confirmed that the spheroid size and structure were kept almost constant after injecting through 23-gauge and 27-gauge needles, whose inner diameters were 400 μm and 230 μm, respectively (Fig. S1). Transgene expression in host mice was evaluated after transplantation of spheroids transfected with luciferase-expressing pDNA. For the control, identical numbers of suspended hepatocytes prepared from a monolayer culture system were transplanted by injection. Luciferase expression in host mice was measured using an IVIS™ imaging system. After subcutaneous transplantation of hepatocytes (spheroids or isolated suspensions) in the abdominal region one day after receiving transfection with luciferase-expressing pDNA, the spheroids showed approximately 10 times higher levels of luciferase expression than those in hepatocytes in suspension form over a period of one month except 4 h after transplantation (Fig. 2). The increase of luciferase expression from

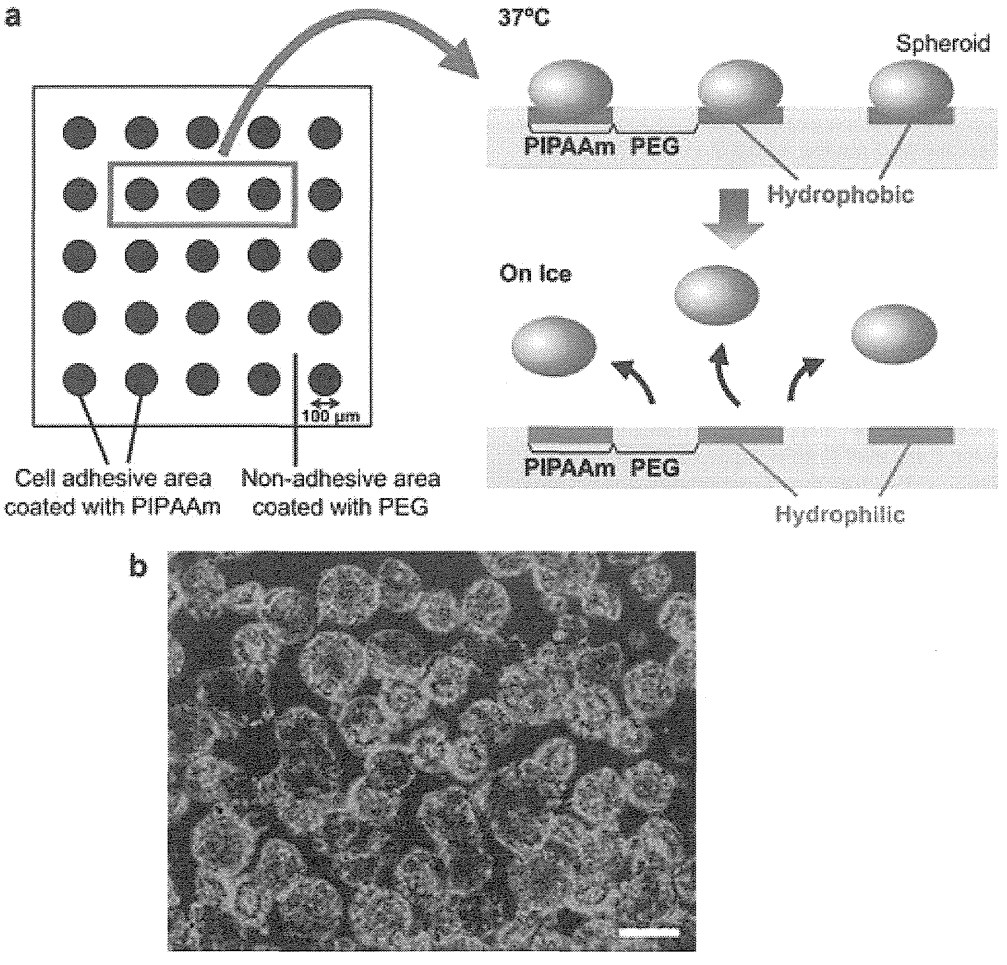

Fig. 1. Preparation of spheroids in the form of homogeneous suspension using thermosensitive micropatterned plate. (a) Scheme of micropatterned plate and mechanism of spheroid recovery. By placing the plate on ice followed by the addition of cold phosphate-buffered saline (PBS), the spheroids were recovered in an injectable suspension form without disrupting their 3D structure. (b) Microscopic image of hepatocyte spheroids dispersed in PBS. Scale bar: 100 μm.

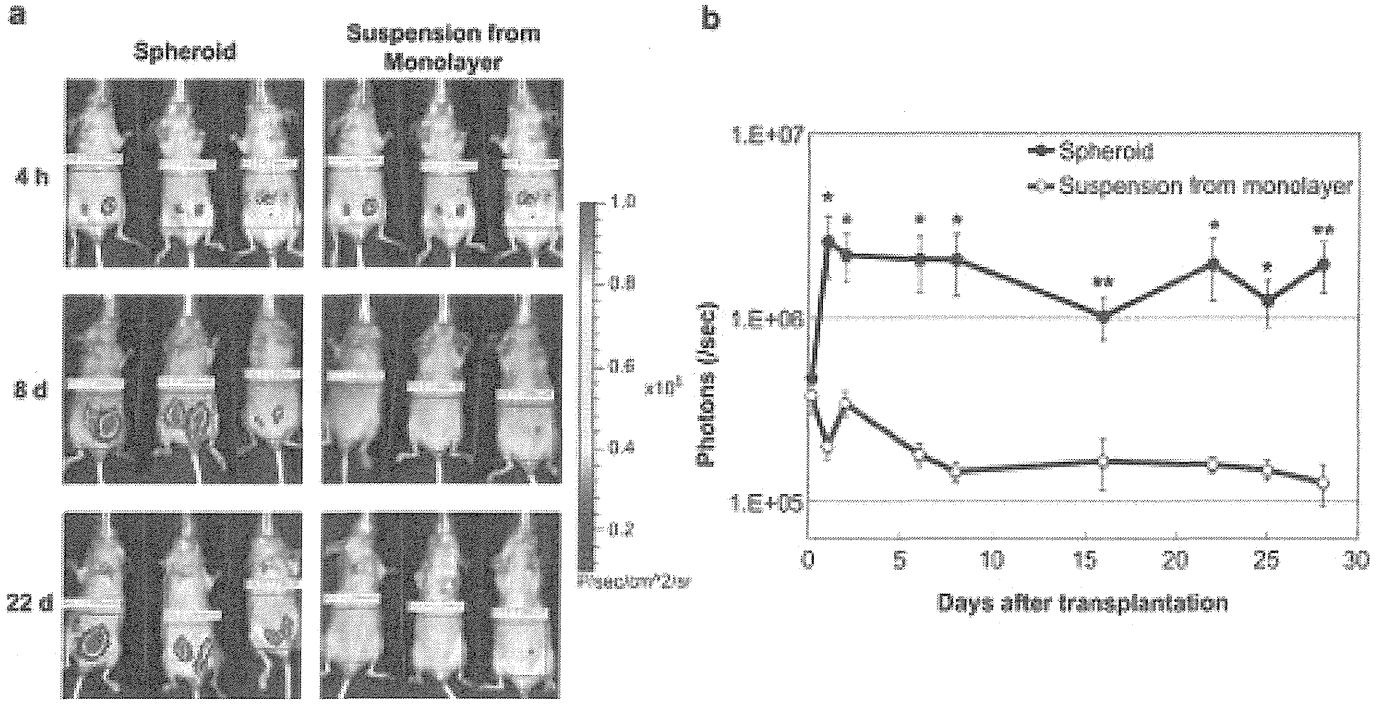

Fig. 2. Luciferase expression in host mice after hepatocyte transplantation. After 24 h of transfection with luciferase-expressing pDNA, hepatocyte spheroids and single-cell suspension from monolayer cultures were transplanted into the subcutaneous tissue of the abdominal region. Luciferase expression in host mice was evaluated using an IVIS™ Imaging System. (a) Representative images of the indicated time point after transplantation, (b) quantification of luminescence intensity. Data are presented as the mean ± standard error of the mean (s.e.m.) ($N = 7$). Statistical significance was assessed by 2-tailed Student's *t*-test, $^{*}p < 0.05$, $^{**}p < 0.01$ versus hepatocytes from monolayer cultures.

4 h to 24 h after transplantation is likely to reflect the time interval required for intracellular processing of pDNA before its expression, such as endosomal escape and nuclear entry. A similar result was obtained for cells transplanted into the subcutaneous tissue of the forelimbs, in which the spheroids yielded higher transgene expression than that in the suspension form 24 h after transplantation, while both showed comparable expression at 4 h (Fig. S2). Thus, the difference in transgene expression between spheroid and monolayer cultures after transplantation became obvious over time. It is interesting to note that hepatocytes in both spheroid and monolayer culture systems exhibited comparable transgene expression of luciferase in *in vitro* culture (Fig. 3). Therefore, the decreased luciferase expression in transplanted hepatocytes in suspension form over time is suggested to be because of a gradual decrease in cell survival or functionality after transplantation, which is in a sharp contrast to the spheroids showing sustained transgene expression.

3.2. Cell survival and distribution in host tissue after transplantation

To obtain more insight into the prolonged transgene expression of cells in spheroids, we examined the survival and function of transplanted hepatocytes in host tissue. The number of vital cells in host tissue was evaluated using quantitative real-time polymerase chain reaction (qRT-PCR) measurements of the copy number of SRY genes on the Y chromosome after collecting total DNA from the host tissue. Using hepatocytes from male rats for cell transplantation into female mice, the number of transplanted cells was determined by discriminating them from host cells [30]. As shown in Fig. 4a, the number of hepatocytes in the host tissue 24 h after transplantation was comparable between the groups of spheroids and single-cell suspension. The transgene copy numbers (luciferase-expressing pDNA) were also comparable between these two groups (Fig. 4b), and even the cells prepared from the monolayer cultured sample showed a relatively high value. Consequently, the enhanced transgene expression in spheroids, as seen in Fig. 1, was not explained by the difference in survival rate of the cells after transplantation.

The albumin expression in host mice was evaluated as a marker of innate hepatocyte function by collecting total mRNA from the transplantation site (forelimb) 24 h after cell transplantation, followed by qRT-PCR analyses to calculate the mRNA expression of

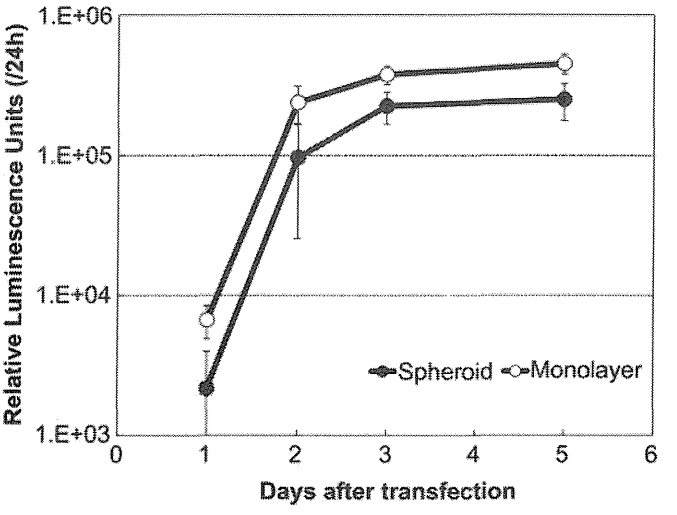

Fig. 3. Luciferase expression after *in vitro* transfection. Hepatocytes in spheroid or monolayer cultures were transfected with a secretory form of luciferase (Gaussia luciferase; Gluc)-expressing pDNA. The values indicate Gluc expression in the last 24 h of each time point because the culture medium was replaced precisely 24 h prior to the measurement. The data are presented as the mean ± standard error of the mean (s.e.m.) ($N = 6$). RLU, relative luminescence unit.